Sensitivity of Tidal Bed Stress Distributions, Near-Bed Currents, Overtides, and Tidal Residuals to Frictional Effects in the Eastern Irish Sea

ALAN M. DAVIES AND JOHN E. JONES

Proudman Oceanographic Laboratory, Bidston Observatory, Birkenhead, Merseyside, United Kingdom

(Manuscript received 11 May 1994, in final form 18 August 1995)

ABSTRACT

A three-dimensional nonlinear high-resolution hydrodynamic model of the eastern Irish Sea is used to examine the influence of near-bed viscosity and bottom friction upon the M_2 tide and overtides in the region.

Initially, bed stress in the model is related to the depth-mean current, the formulation used in a "classic" two-dimensional model. The resulting hybrid "two-dimensional/three-dimensional model" enables changes in current profile due to variations in eddy viscosity to be examined independently of those due to changes in bed stress. Also, results from the model are compared with those from a three-dimensional model with bed stress related to bottom current.

Computed tidal elevations and surface currents are found to be fairly insensitive to the parameterization of bottom stress. However, tidal current profiles in the near-bed region and maximum bed stress are found to be sensitive to variations in near-bed viscosity and friction coefficient. Although reducing eddy viscosity in the near-bed region and increasing bottom frictional coefficient makes little difference to tidal elevations and near-surface tidal currents, it is essential to accurately reproduce the bed currents and associated bed stress.

Higher harmonics of the tide (the overtides) computed with the model show significant spatial variability in the region, with near-bed currents being influenced by frictional effects. Tidal residual flows also show significant spatial variability with near-bed flows being influenced by friction.

1. Introduction

Over the last twenty years two-dimensional hydrodynamic tidal models have become well established and are used for a number of tidal simulations, ranging from full basin oceanic tidal models (e.g., Schwiderski 1986), to limited regions of the ocean (e.g., Flather et al. 1994, personal communication), to shallower water situations (Lynch and Werner 1991; Werner and Lynch 1989), and estuaries (Uncles 1991). In these two-dimensional models, the main emphasis has been on tidal elevations, although in recent years interest has focused on tidal currents; in particular near-bed currents both at the fundamental, higher harmonics and residuals responsible for sediment movement, and tidally generated turbulence, which in shallow seas is a major source of mixing.

Well-established finite difference methods on regular meshes have in general been used in the horizontal, although boundary fitted coordinates (e.g., Spaulding 1984) and recently the finite element method (e.g., Lynch and Naimie 1993; Foreman et al. 1990, 1993) with its ability to grade the mesh have become more popular.

In recent years with the rapid increase in computer power, high-resolution three-dimensional hydrodynamic modeling has been possible, and a number of three-dimensional models have been developed (e.g., Blumberg and Mellor 1987; Davies and Jones 1990, 1992; Gordon and Spaulding 1987; Lynch and Naimie 1993; Lynch and Werner 1990, 1991; Luyten et al. 1994; Heaps and Jones 1981; Johns et al. 1992; Johns and Xing 1993) with the prime aim of examining current profiles.

In parallel with these developments in numerical modeling, significant progress has been made with a range of instruments designed to measure currents in the vertical, (e.g., acoustic Doppler current meters) and, in particular, near-bed currents and turbulence intensities (e.g., Green et al. 1990; Lohrmann et al. 1990; Crawford 1991), which are important in a large number of shallow sea problems. Bed stress and bed turbulence are particularly large in shallow water regions with strong tidal currents, such as the eastern Irish Sea (Fig. 1), with water depths varying from 50 m offshore to less than 10 m in a large nearshore region.

The high-resolution eastern Irish Sea topography and grid of Aldridge and Davies (1993), used previously to examine the M_2 tide in the region, is employed to investigate the spatial variability and processes influ-

Corresponding author address: Dr. Alan M. Davies, Proudman Oceanographic Laboratory, Bidston Observatory, Birkenhead, Merseyside L43 7RA, United Kingdom.

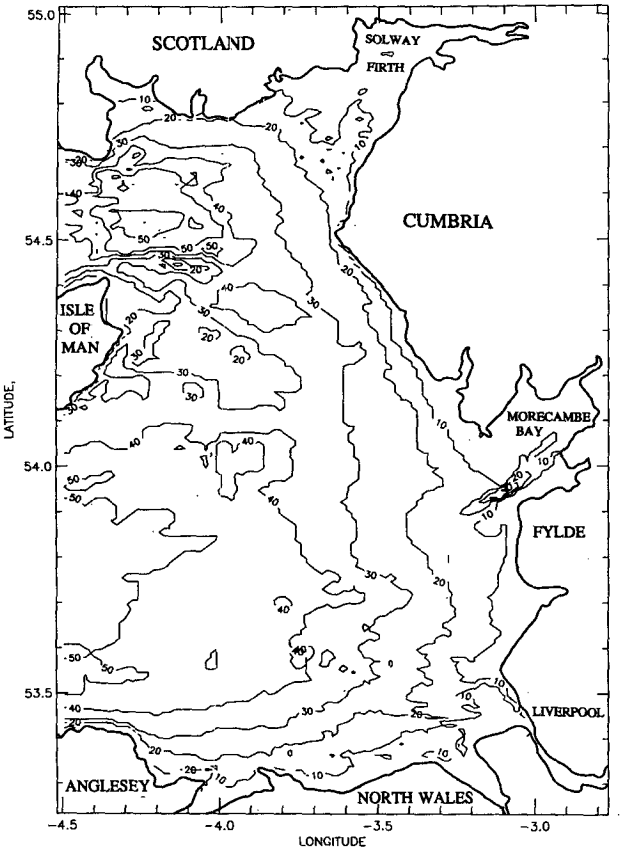

FIG. 1. Schematic of various geographical locations and bottom topography of the eastern Irish Sea.

encing higher tidal harmonics (overtides) and tidal residuals in the area. In previous calculations (Aldridge and Davies 1993), eddy viscosity, although varying with the flow field, was maintained constant in the vertical and a slip condition was used at the seabed. Aldridge and Davies (1993) found that, although this formulation of viscosity and friction yielded accurate currents in the upper part of the water column, the current at the bed was overestimated. In a subsequent series of calculations, using a coarse grid model of the Irish Sea with a no-slip condition at the seabed, Davies (1993) was able to reproduce the near-bed M_2 tidal current. However, the use of a no-slip condition excludes the application of a time-split approach and in a fine grid model would be computationally expensive. In the present series of calculations we examine if comparable current accuracy to that found with the no-slip condition (Davies 1993) can be obtained using a slip condition, with the associated computational saving in time using a time-splitting method. The influence of near-bed viscosity and bottom friction coefficient upon current profiles is also examined. In the series of calculations described here, we also examine the effects of friction in the near-bed region upon fundamental and higher harmonics. A linear decrease in viscosity close to the seabed, together with a range of friction coefficients, is considered in these calculations. The effect of this upon bed-stress distributions is also examined.

The M_2, M_4, and M_6 tides in the eastern Irish Sea are determined, using a regular finite difference grid in the horizontal (Figs. 2a,b) with a grid resolution of the order of 1 km [an identical grid to that used by Aldridge and Davies (1993) to examine the M_2 tide]. By using a grid having such a fine resolution, it is possible to resolve in detail the nonlinear terms responsible for generating the higher tidal harmonics. Comparisons of computed and observed elevations are made at 24 offshore and shore-based tide gauges, and 61 current meter analyses [a larger dataset than that used by Aldridge and Davies (1993)].

2. Numerical model

The fully nonlinear three-dimensional hydrodynamic equations used in the model have been given previously in Aldridge and Davies (1993).

Along closed land boundaries the normal component of current is set to zero. However, in the very shallow water regions that can be resolved with the present model, areas flood and dry during various stages of the tidal cycle, and to allow for this a dynamic lateral boundary condition is also used (Aldridge and Davies 1993; Flather and Hubbert 1990). At open boundaries a radiation condition is applied (Davies 1986) with M_2, M_4, and M_6 tidal elevation and current input taken from large area coarser grid models of the region (Davies and Jones 1992).

At the sea surface, a zero stress boundary condition is applied, while at the seabed a slip condition is used. In a three-dimensional model the bed-stress components F_B and G_B are given by

$$F_B = -\rho\left(\mu \frac{\partial u}{\partial z}\right)_h, \quad G_B = -\rho\left(\mu \frac{\partial v}{\partial z}\right)_h \qquad (1)$$

and can be evaluated by a number of methods. In a two-dimensional vertically integrated model where only the depth mean currents $\bar{u}$ and $\bar{v}$ are available, use of a quadratic friction formulation yields

$$F_B = k\rho\bar{u}(\bar{u}^2 + \bar{v}^2)^{1/2}, \quad G_B = k\rho\bar{v}(\bar{u}^2 + \bar{v}^2)^{1/2} \qquad (2)$$

with k a friction coefficient relating bed stress to the depth mean current, h water depth, and z the vertical coordinate.

In a three-dimensional model, the depth-mean currents are also computed, and hence equation (2) can be used. However, since the bed currents are also determined, then it is common (e.g., Davies 1986) to use

$$F_B = K\rho u_h(u_h^2 + v_h^2)^{1/2}, \quad G_B = K\rho v_h(u_h^2 + v_h^2)^{1/2}. \qquad (3)$$

In these equations, ρ denotes the density of sea water, with μ vertical eddy viscosity, u and v the east and north

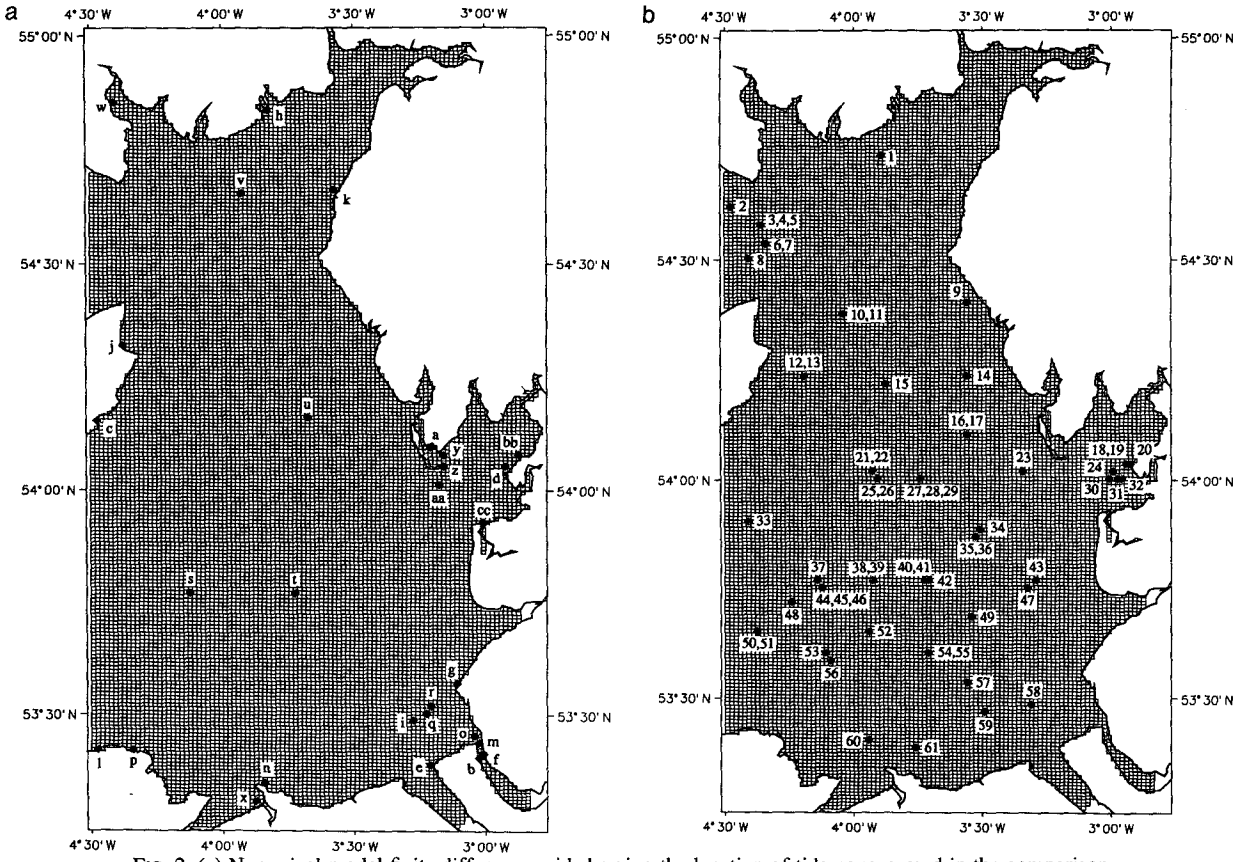

FIG. 2. (a) Numerical model finite difference grid showing the location of tide gauges used in the comparison. (b) As in Fig. 2a but showing the location of current observations used in the comparisons.

components of velocity, and u_h and v_h the bed currents, with K the friction coefficient that relates the bed stress to the current. In Aldridge and Davies (1993) K was given by a C_{100} value (where C_{100} is the coefficient that relates the bed stress to the current 100 cm above the bed), with eddy viscosity assumed constant in the vertical. However, Davies (1990) showed that in the near-bed region eddy viscosity decreases very rapidly with the friction coefficient increasing as the near-bed layer is approached. As we will show subsequently by using a viscosity profile that decreases in the near-bed region with a friction coefficient higher than the conventional C_{100} value, near-bed currents can be computed with a significantly greater accuracy than using a constant eddy viscosity profile. Also, the method has a substantial computational advantage over the use of a no-slip bottom boundary condition (Davies 1993) in that a time-split integration method can also be used (see section 3).

In subsequent calculations to determine the influence of bed friction coefficient and near-bed viscosity upon tidal elevations and current profiles, we will initially determine the bed stress using the parameterization applied in a two-dimensional model, namely Eq. (2), in the three-dimensional model. This hybrid two-dimensional/three-dimensional model is interesting in that it yields identical tidal elevations for a given friction coefficient k as does a two-dimensional model, although the tidal current profile varies with changing viscosity profile. By this means, changes in current profile due to viscous effects can be examined independently of those due to frictional effects and the resulting changes in tidal elevation, which occur in a full three-dimensional model where the bed stress is computed from Eq. (3).

3. Numerical solution and eddy viscosity formulation

a. Formulation of a mixed finite difference–spectral model

The numerical methods used to solve the three-dimensional hydrodynamic equations have been presented in detail elsewhere (Davies 1986, 1987) and only the major features are outlined here.

A standard Arakawa C grid is used in the horizontal with surface elevation ζ, and the u and v components

of velocity evaluated at different grid points, namely, on a staggered grid. The finite difference grid has a resolution of 0.5′ north–south, giving a spacing of order 0.9 km, and 1.0′ west–east, a resolution of order 1.0 km. The region covered by the model is shown in Figs. 2a,b, which also shows the location of tide gauges and current meters used in subsequent comparisons. The open boundary of the model where tidal forcing is applied extends due north and south from the Isle of Man.

Discretization in the vertical is accomplished by first transforming the equations to sigma coordinates (Davies 1986), defined by

$$\sigma = (z + \zeta)/(h + \zeta). \tag{4}$$

By this means a surface and seabed boundary-following coordinate system is obtained, enabling the physics of the bottom boundary layer to be accurately resolved; a significant advantage over the use of a standard z coordinate with the associated problems of representing the near-bed region.

The two components of velocity u and v are expanded in terms of a set of basis functions $f_r(\sigma)$ through the vertical and coefficients $A_r(\chi, \phi, t)$ and $B_r(\chi, \phi, t)$ varying with horizontal position and time, giving

$$u(\chi, \phi, t) = \sum_{r=1}^{m} A_r(\chi, \phi, t) f_r(\sigma)$$

$$v(\chi, \phi, t) = \sum_{r=1}^{m} B_r(\chi, \phi, t) f_r(\sigma) \tag{5}$$

with χ longitude, ϕ latitude, and t time.

In the calculations described subsequently eddy viscosity μ is expressed as

$$\mu = \alpha(\chi, \phi, t)\Phi(\sigma), \tag{6}$$

with α a coefficient, which determines the magnitude of the eddy viscosity and is related to the flow field, and $\Phi(\sigma)$ a specified function in the vertical. For the case of a fixed $\Phi(\sigma)$ there are significant computational advantages in taking the functions $f_r(\sigma)$ to be the eigenfunction (modes) of the eddy viscosity profile, subject to a slip condition at the seabed (Davies 1986, 1987). By this means the first mode represents the depth-mean current, and all the higher modes, which are orthogonal to it, only contribute to the current profile and are not involved in the continuity equation (Davies 1987). That the higher modes do not contribute to the continuity equation means that a time-splitting integration method can be adopted in which the first mode is integrated with a short time step (t^*) determined by the CFL condition. The higher modes and the advective terms (which represent the major computational effort) are then evaluated with a much longer time step $\Delta t = nt^*$, and in the calculation described here, n was taken as 24, with t^* of order 24.5 sec, giving $\Delta t = 588$ sec.

b. Eddy viscosity parameterization

In a previous series of calculations using a large area coarse grid model of the Celtic and Irish Seas with five tidal constituents (Davies and Jones 1992), a successful parameterization of eddy viscosity was of the form,

$$\mu = K_2(\bar{u}^2 + \bar{v}^2)^{1/2}\Delta, \tag{7}$$

with Δ the bottom boundary layer thickness given by

$$\Delta = \frac{CU_*}{\omega_1}, \tag{8}$$

where U_* is the instantaneous bed friction velocity, $K_2 = 0.0025$ and $C = 0.3$ are specified coefficients, and ω_1 is a characteristic frequency taken as the M_2 tidal frequency. In shallow water regions, such as the eastern Irish Sea, the boundary layer thickness is depth-limited; consequently $\Delta = h$, giving

$$\mu = K_2(\bar{u}^2 + \bar{v}^2)^{1/2}h. \tag{9}$$

Using a turbulence energy model Davies and Jones (1990) found that in the eastern Irish Sea the turbulent bottom boundary layer extends to the sea surface over the majority of the region and that in this region eddy viscosity could be determined from Eq. (9). This parameterization was also used by Aldridge and Davies (1993).

Two simple idealized eddy viscosity profiles are considered in the vertical. In the first (profile A), eddy viscosity is constant from sea surface to seabed; this is the profile used by Aldridge and Davies (1993). In the second (profile B), eddy viscosity is constant at a value μ_1 in the upper part of the water column, decreasing linearly to a value μ_0 at the seabed over a bottom boundary layer of thickness $h_1 = \beta h$ with β a specified coefficient.

The reason for choosing such an idealized profile is that it reflects the linear decrease in eddy viscosity in the near-bed region, which is known from boundary layer theory and also appears in tidal eddy viscosity profiles computed with turbulence energy models (Davies 1991). Obviously, a more complex profile such as the near-parabolic profile found in turbulence models (Davies 1991) could be used. However, as shown previously (Davies 1991, 1993), the profile of eddy viscosity in the upper part of the water column does not influence tidal currents since in this region the vertical variation of the tide is small, and hence its product with the eddy viscosity is not significant and a depth-independent value is appropriate.

In the lower part of the water column, turbulence energy models (Davies 1991) show eddy viscosity increasing in a nearly linear manner with height above the seabed. In order to clearly demonstrate the effects of bed-friction coefficient, bed viscosity, and height above the bed over which a linear decrease is appropriate, the idealized viscosity profile B is used rather

TABLE 1. Overview of parameters used in the various calculations (the letter L following the calculation number indicates that advection was omitted).

Calculation	Friction k	Friction K	μ Profile	μ_0	β	Depths
1	0.0018	—	A	—	—	Original
2	—	0.00375	A	—	—	Original
2L	—	0.00375	A	—	—	Original
3	—	0.00375	A	—	—	1.10 × Original
4a	—	0.01125	B	0.2	0.5	Original
4b	—	0.01125	B	0.2	0.1	Original
4L	—	0.01125	B	0.2	0.1	Original
5a	—	0.01125	B	0.04	0.1	Original
5b	—	0.03375	B	0.04	0.1	Original

than a more complex profile in which the role of the various parameters cannot be clearly understood. This idealized viscosity profile is consistent with one of those used by Davies (1993) with a no-slip condition, enabling comparisons to be made between slip and no-slip models.

4. Tidal calculations

a. Hybrid 2D/3D model

In an initial calculation (calc 1 in Table 1), the hybrid two-dimensional/three-dimensional model was run with bottom stress determined from the depth mean current, with $k = 0.00187$, and the eddy viscosity profile constant in the vertical (profile A), for a magnitude determined from Eq. (9). Since the bed stress is computed from the depth mean current, then surface elevations and depth mean currents are identical to those computed with a conventional two-dimensional model, and the parameterization of eddy viscosity only influences the current profile in the vertical.

The M_2 cotidal chart (Fig. 3) computed with the model was not significantly different from that determined by Aldridge and Davies (1993) using a three-dimensional model and shows the characteristic features (Robinson 1979) of the tide in this region; namely, tidal amplitudes increasing from west to east as the tide propagates into the shallow eastern Irish Sea, with phase increasing from south to north. Comparison of differences between computed and observed M_2 tidal amplitudes at a number of coastal and offshore tide gauges (Table 2) shows that at the majority of locations tidal amplitude can be determined to within 10 cm. At two locations, namely Ramsey and Formby, there are significant errors; however, similar errors at these locations have been found in other models [e.g., Davies and Gerritsen (1994), who report that the analysis at these ports is based on very short spans of data and may be prone to error]. At location (i), an offshore tide gauge in Liverpool Bay, there is an appreciable error of order 30 cm. However, at two nearby locations (q) and (r), the model agrees to within 5 cm of the observed, suggesting a local feature that the model cannot resolve or an error in the observations at location (i). A similar discrepancy occurs at position (z), although at nearby locations (aa) and (y) the model is in good agreement with the observations, suggesting that the observed results at location (z) may be of limited use. In very shallow locations, positions (w) and (x), local features not resolved by the model may have an influence leading to the errors in amplitude of the order of 20 cm.

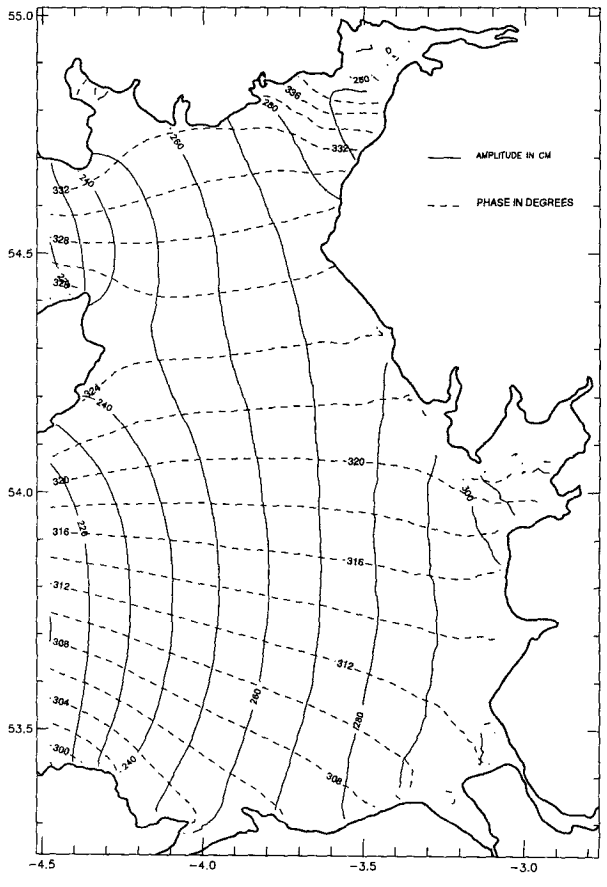

FIG. 3. Computed M_2 cotidal chart determined with the hybrid 3D/2D model (calc 1 in Table 1).

TABLE 2. Comparison of errors $\Delta\zeta$ (cm) in amplitude and Δg (deg) in phase for the M_2 tide.

		Observed		Run 1		Run 2		Run 3		Run 4a		Run 4b		Run 5a		Run 5b	
Point	Port	ζ_0	g_0	$\Delta\zeta$	Δg	$\Delta\zeta$	Δg	$\Delta\zeta$	Δg	$\Delta\zeta$	Δg	$\Delta\zeta$	Δg	$\Delta\zeta$	Δg	$\Delta\zeta$	Δg
a	Barrow	308	331	6	−5	4	−3	15	−8	5	−1	1	1	1	1	−5	4
b	Birkenhead	311	323	−2	−9	−3	−8	5	−12	−5	−6	−6	−4	−7	−5	−9	−1
c	Douglas	230	326	0	−2	−0	−2	13	−6	−2	−3	−5	−2	−4	−3	−7	−2
d	Heysham	315	325	4	−3	6	−2	13	−7	6	−1	2	1	2	1	−3	4
e	Hilbre	292	317	7	−5	7	−4	15	−8	7	−4	5	−2	6	−3	4	−0
f	Liverpool	312	323	−5	−8	−4	−6	3	−11	−7	−5	−7	−3	−9	−4	−10	−1
g	Formby	312	315	−14	−2	−14	−2	−6	−5	−15	−1	−17	−0	−17	−1	−17	1
h	Hestan	275	339	5	−4	2	−4	14	−8	−2	−3	−8	−2	−6	−3	−13	−1
i	Liverpool Bay	262	315	30	−3	30	−3	39	−6	31	−2	28	−1	29	−2	27	0
j	Ramsay	262	328	−18	−3	−19	−3	−5	−7	−22	−3	−24	−2	−24	−3	−27	−2
k	Workington	273	332	10	−2	8	−1	20	−6	4	−1	−1	−0	1	−1	−5	0
l	Wylfa Head	206	300	2	−2	2	−3	13	−3	2	−4	2	−5	2	−5	2	−6
m	Liverpool	307	321	−2	−7	−1	−6	8	−10	−2	−5	−5	−2	−5	−3	−5	0
n	Llandudno	267	308	−1	−3	−1	−2	9	−4	−1	−3	−2	−1	−2	−2	−3	−1
o	New Brighton	306	318	−0	−4	−0	−3	7	−7	−3	−2	−3	−0	−5	−1	−4	2
p	Amlwch	235	305	−6	−4	−6	−4	4	−5	−6	−5	−6	−5	−7	−5	−7	−5
q	Ost G	290	315	4	−3	5	−3	13	−6	5	−2	2	−1	3	−1	1	0
r	Queens Channel	296	316	−1	−3	−0	−3	7	−6	0	−3	−3	−1	−3	−2	−4	0
s	STD Irish Sea	235	317	2	−4	1	−4	13	−7	0	−4	−1	−4	−1	−5	−2	−4
t	Stn10	262	318	2	−4	2	−3	12	−6	2	−3	−0	−2	0	−3	−1	−2
u	Stn34	263	324	5	−3	4	−2	16	−6	3	−2	−0	−1	0	−2	−2	−0
v	Stn35	255	332	9	−2	7	−2	20	−6	3	−2	−1	−1	0	−2	−4	−1
w	Creetown	233	342	20	−5	17	−4	34	−10	15	−3	11	−2	13	−3	6	−0
x	Conwy	241	318	20	−13	21	−13	30	−15	21	−13	19	−12	20	−13	19	−12
y	Barrow RI	306	329	6	−4	6	−3	15	−8	6	−1	0	1	1	1	−5	4
z	Barrow HP	292	327	19	−2	19	−1	26	−6	18	1	13	2	13	2	7	5
aa	Barrow HS	297	325	4	−4	4	−3	13	−7	2	−2	−0	−1	−1	−2	−3	0
bb	Morecambe	308	326	−0	−1	−2	0	14	−4	2	3	−5	6	−4	5	−18	10
cc	Fleetwood	305	326	8	−6	8	−5	17	−9	5	−4	2	−2	2	−3	0	−0

Phase errors (Table 2) show a bias in the model with the phase, on average, underpredicted by the order of 5°. The slight bias in the model to overpredict elevations, with 14 ports where elevation is overpredicted by up to 10 cm as compared to 8 ports where it is underpredicted, is clearly evident from the histogram of errors (Table 3a). Similarly there are 21 locations at which the phase is underpredicted by 5°. Root mean square (rms) errors (Table 3a) of 10.7 cm and 5.3° suggest that, despite the large discrepancy between observed and computed results at a number of ports, the model has a sufficiently fine grid to represent the nearshore tidal variations. The phase error of order 5° at all locations is directly related to the open boundary input (Aldridge and Davies 1993) and could be removed by a phase change in boundary input.

Besides computing the rms errors in amplitude and phase, a measure of the overall performance of the model can be determined by computing the error H_s at each port where H_s is given by

$$H_s = \{(H_1)^2 + (H_2)^2\}^{1/2},$$

with

$$H_1 = H_0 \cos(g_0) - H_c \cos(g_c)$$

$$H_2 = H_0 \sin(g_0) - H_c \sin(g_c),$$

where H_0, g_0 is the observed amplitude and phase with H_c, g_c the computed. The values of H_s are then summed over all ports giving the total H_s value shown in Table 3a of 734 cm. Since H_s is a single value representing the overall error in the computation, reducing the value of H_s represents an increase in overall accuracy of the calculation.

The spatial distribution of M_2 tidal currents computed with the hybrid model is also similar to that found by Aldridge and Davies (1993), using a full three-dimensional model with strong rectilinear currents, having the major axis aligned in a west–east direction close to the open boundary of the model, with a region of weaker tidal currents of a more circular tidal current ellipse between the Isle of Man and the Cumbrian coast (a more detailed discussion of tidal currents in relation to bed stress will be presented later in connection with the full three-dimensional model).

Although the spatial distribution of tidal current ellipses is, in general, in agreement with observations (Howarth 1990) and previous models (Aldridge and Davies 1993), the critical test of the model is its ability to accurately reproduce tidal current magnitudes and current shear in the region. Comparing computed and observed tidal current ellipse parameters in detail at a number of locations taken from those shown in Fig. 2b, it is possible to determine any deficiencies in the model's ability to compute tidal current profiles. Comparing the magnitude of computed and observed tidal current ellipses at location 2, close to the model's open boundary, it is clear that the major axis is overpredicted by the order of 16 cm s^{-1} at this location, although farther east at positions 3, 4, and 5, near-surface current ($\sigma = 0.38$) is accurately determined, although the near-bed ($\sigma = 0.92$) current is overpredicted. Similarly, at

TABLE 3a. Number of points where computed elevation amplitude or phase exceeds (+) or is below (−) the observed value: amplitude h (in cms), phase g (in deg).

Calculation		−20	−15	−10	−5	+5	+10	+15	+20	rms	H_s
						M_2 tide					
1	h	1	1	1	7	7	7	1	2	10.7 cm	734
	g	0	1	7	21	0	0	0	0	5.3°	
2	h	1	1	1	8	7	7	0	2	10.5 cm	636
	g	0	1	4	23	1	0	0	0	4.6°	
3	h	0	0	2	0	3	4	9	5	17.3 cm	1212
	g	1	4	21	3	0	0	0	0	7.9°	
4a	h	1	0	3	6	8	6	0	2	10.3 cm	531
	g	0	1	2	24	2	0	0	0	4.0°	
4b	h	1	0	7	9	6	1	2	1	9.8 cm	456
	g	0	1	2	21	4	1	0	0	3.6°	
5a	h	1	0	5	7	10	1	2	1	9.8 cm	468
	g	0	1	1	22	4	1	0	0	3.7°	
5b	h	2	2	7	10	3	2	0	1	10.7 cm	486
	g	0	1	2	14	10	1	1	0	4.0°	
						M_4 tide					
4a	h	0	1	3	8	14	2	0	0	6.1 cm	261
	g	3	4	0	3	2	1	0	0	30.4°	
4b	h	0	1	5	5	15	2	0	0	6.0 cm	253
	g	4	4	1	3	2	1	0	0	29.4°	
4L	h	1	1	5	10	9	2	0	1	6.4 cm	254
	g	4	4	1	2	3	0	0	2	31.4°	

TABLE 3b. Number of current meter analysis where computed semimajor axis (A) exceeds (+) or is below (−) the observed value (in cm s^{-1}).

Calculation		−20	−15	−10	−5	+5	+10	+15	+20	rms
					M_2 tide					
1	A	0	1	2	4	16	32	14	8	10.7 cm s^{-1}
2	A	0	1	2	5	21	25	16	6	10.4 cm s^{-1}
3	A	0	3	1	11	32	17	13	1	8.0 cm s^{-1}
4a	A	0	1	1	11	17	21	13	12	11.3 cm s^{-1}
4b	A	1	3	9	13	12	19	15	5	11.1 cm s^{-1}
5a	A	1	0	4	12	16	25	12	6	10.5 cm s^{-1}
5b	A	1	0	6	12	17	22	14	6	10.3 cm s^{-1}
					M_4 tide					
4a	A	0	0	2	18	56	3	0	0	2.4 cm s^{-1}
4b	A	0	0	1	26	50	2	0	0	2.1 cm s^{-1}
4L	A	0	0	0	36	42	1	0	0	2.0 cm s^{-1}
2L	A	0	0	1	34	42	2	0	0	2.2 cm s^{-1}

locations 6 and 7 the model appears to accurately predict near-surface, although not nearbed currents. Farther south at locations 33, 50, and 51 there appears to be a bias in the model. A detailed discussion of this will be presented later in connection with the determination of bed stress from the near-bed currents.

At locations to the east of the Isle of Man (positions 12, 13) tidal current velocity is significantly lower, and the more circular nature of the tidal current ellipse found in the observations is accurately reproduced in the model, although again the model overpredicts the near-bed currents. Similar good agreement between model and observations is found farther eastward at locations 16 and 17 and position 23, although the model still has a tendency to overpredict the tidal current in the nearbed region.

Farther south at locations 44, 45, 46 and adjacent location 37 (where there is a near-bed measurement) it is evident that the model slightly overpredicts (by order 7 cm s^{-1}, a 10% error) the magnitude of the near-surface tidal current ellipse, although the near-bed current at location 37 is significantly overpredicted (65 cm s^{-1} compared with 40 cm s^{-1}). Similarly, at locations 50 and 51 the observed shear between the two observations of 24 cm s^{-1} is underestimated in the model, which produces 11 cm s^{-1}. In general, the orientation of the major axis of the current ellipse is reproduced by the model to within 10°. From the histogram of errors of the semimajor axis (Table 3b) and the rms error, it is apparent that there is a bias in the model that tends to overpredict tidal currents by the order of 10 cm s^{-1}.

b. Three-dimensional model (eddy viscosity profile A)

In a subsequent calculation using the full three-dimensional model (calc 2, Table 1), the bed stress is computed from the bed current. In this calculation a larger value of bottom friction was used, $K = 0.00375$, corresponding to a C_{100} value. Open boundary input to the model and water depths were identical to those used in calculation 1. Errors in computed elevation and phase (Table 2) are slightly reduced in the three-dimensional calculation, giving a reduction in the rms error and the H_s error (indicating a more accurate solution) and a slight change in the histogram of errors (Table 3a).

Comparing tidal current ellipse parameters (Table 3b), there has been a small reduction in the rms error in the major axis of the current ellipse with a slight change in the histogram of errors (Table 3b), giving 26 points where the computed major axis is to within 5 cm s^{-1} of observed, compared with 20 in the case of the hybrid model. A detailed comparison of current ellipse parameters (Table 4) shows that although near-surface currents in the three-dimensional model are only slightly different (of order 1 cm s^{-1} larger) than in the hybrid model, near-bed currents are reduced by the order of 3 cm s^{-1}, giving rise to better agreement with the observations. This result is particularly interesting in that the same eddy viscosity formulation was used in both models, and suggests that the improvement in near-bed currents is due to using a bed stress related to the bottom current and not the depth mean. In essence, this improvement in current structure is due to a better representation of the bed stress rather than internal friction effects, namely, eddy viscosity which was not changed.

In a third calculation, aimed at examining the sensitivity to water depths, the previous calculation was repeated but with all water depths increased by 10%. Increasing the water depths effectively reduces the effects of bottom friction in that the retarding force is the bed stress divided by water depth, giving rise to an increase in surface elevation amplitudes (Table 2), with a resulting increase in the error in the model (Table 3a). This change in water depth does, however, lead to a reduction in currents at all depths (Table 4)

TABLE 4. Comparison of observed and computed semimajor axis A (cm s^{-1}), orientation T (deg), and rotation R of the M_2 tidal current ellipse at a number of depths and locations.

	Obs			Calc 1			Calc 2			Calc 3			Calc 4a			Calc 4b			Calc 5a			Calc 5b			h	
Rig	A_0	T_0	R_0	A_c	T_c	R_c	A_c	T_c	R_c	A_c	T_c	R_c	A_c	T_c	R_c	A_c	T_c	R_c	A_c	T_c	R_c	A_c	T_c	R_c	(m)	σ
2	110	9	−	126	12	+	126	12	+	120	12	+	127	12	+	126	11	+	126	11	+	126	11	+	52	0.30
3	97	7	+	100	11	+	101	11	+	96	11	+	103	9	+	104	11	+	104	10	+	107	11	+	48	0.38
4	91	10	+	99	11	+	100	11	+	94	12	+	102	10	+	101	11	+	100	9	+	104	11	+		0.44
5	62	14	+	79	12	+	75	13	+	71	13	+	60	13	+	61	14	+	64	12	+	52	15	+		0.92
6	86	171	+	89	184	+	90	184	+	85	184	+	91	182	+	91	183	+	91	183	+	95	183	+	53	0.42
7	66	174	+	73	185	+	70	185	+	67	185	+	62	185	+	60	186	+	62	185	+	55	187	+		0.88
12	32	46	+	35	35	+	34	34	+	33	36	+	34	33	+	33	31	+	33	33	+	32	30	+	30	0.56
13	29	57	+	32	35	+	30	35	+	29	37	+	29	35	+	27	33	+	28	34	+	25	32	+		0.82
15	37	38	+	39	37	+	38	36	+	37	38	+	37	35	+	34	34	+	37	34	+	32	32	+	23	0.78
16	35	168	+	36	187	+	37	186	+	35	189	+	38	184	+	38	185	+	38	185	+	40	184	+	22	0.40
17	30	172	+	33	188	+	32	187	+	30	191	+	32	186	+	30	187	+	31	187	+	29	187	+		0.78
23	49	148	+	48	159	+	48	159	+	45	159	+	49	159	+	46	160	+	46	160	+	44	161	+	20	0.60
33	79	18	−	92	22	+	94	21	+	89	23	+	97	22	+	97	21	+	97	22	+	100	20	+	60	0.36
37	40	6	+	65	8	+	61	8	+	58	9	+	40	10	+	45	9	+	46	10	+	32	10	+	47	0.98
44	75	5	−	82	5	−	83	5	−	79	6	−	86	5	−	84	4	−	84	4	−	85	4	−	46	0.48
45	72	3	−	79	6	−	79	5	+	75	6	+	80	5	+	77	5	+	77	3	+	75	5	+		0.62
46	66	6	−	73	6	+	71	6	+	68	7	+	70	6	+	65	6	+	68	6	+	62	6	+		0.80
50	89	7	−	98	5	−	99	5	−	95	6	−	101	4	−	101	5	−	101	5	−	104	5	−	57	0.40
51	65	8	−	81	6	+	78	6	+	75	8	+	72	7	−	68	8	+	71	8	−	63	8	+		0.86
56	79	175	−	86	175	−	86	175	−	82	176	−	89	175	−	86	174	−	87	175	−	87	174	−	46	0.50
60	58	169	−	63	169	+	63	169	+	61	169	+	65	168	+	62	168	+	63	168	+	62	167	+	28	0.50
61	48	166	+	52	166	+	50	166	+	48	166	+	50	166	+	46	166	+	48	166	+	43	166	+	20	0.76

with an improvement in the accuracy of the computed currents (Table 3b). The significant increase in error in the elevations does, however, suggest that this improvement in currents is artificial. Also increasing the water depth does not improve the accuracy of the computed shear in the vertical; the model still does not reproduce the observed decrease in current in the near-bed region.

c. Three-dimensional model (eddy viscosity profile B)

Calculations using both no-slip models and turbulence energy models (Davies 1991, 1993) have shown that eddy viscosity decreases in the near-bed region, with a corresponding increase in the friction coefficient to maintain the same bed stress. To reproduce this effect, viscosity profile B was used in the vertical with viscosity decreasing at the seabed to a value μ_0.

In an initial calculation (calc 4a, Table 1), a value of μ_0 was taken as 0.2 times the value μ_1 applied in the upper part of the water column, (i.e., a μ_1:μ_0 ratio of 1:0.2) with the mean value of μ computed from Eq. (9). This reduction in μ means that the reference height at which the drag coefficient is being computed has been reduced, and to allow for this and to be consistent with previous models (Davies 1991, 1993) K was increased by a factor of 3 to $K = 0.01125$ (calc 4a, Table 1). [A detailed discussion of this is presented in Davies (1991, 1990).] The height above the seabed over which the linear decrease in eddy viscosity was assumed to apply was initially set at that used in Davies (1993), namely, $h_1 = 0.5$ h; thus $\beta = 0.5$ (calc 4a, Table 1).

Considering initially M_2 tidal elevation errors, it is evident from Tables 2 and 3a that the error is slightly less than that determined with the 3D model and viscosity profile A (compare calcs 2 and 4a) with H_s being reduced from 636 cm (3D viscosity profile A) to 531 cm (Table 3a).

From a comparison of tidal current ellipse parameters (Table 4), at locations 3, 4, and 5 the semimajor axis near the surface ($\sigma = 0.38$) has slightly increased compared to calculation 2, although close to the bed ($\sigma = 0.92$) it has decreased significantly to a value slightly below the observed value. The orientation of the semimajor axis is also in good agreement with observations (compare calc 4a with observations in Table 4). A similar change (compare calc 4a and calc 2 in Table 4) is evident in the near-bed ($\sigma = 0.88$) semimajor axis at positions 6 and 7, although there is no significant change at positions 16 and 17.

At location 37 the near-bed ($\sigma = 0.98$) current decreases from 61 cm s^{-1} (calc 2) to 40 cm s^{-1} (in perfect agreement with observations), although at location 46 the near-bed ($\sigma = 0.8$) is only reduced by 1 cm s^{-1}.

Considering the histogram of currents (Table 3b), the bias found in calculation 2 is reduced, although the currents are still overpredicted. In a subsequent series of calculations designed to examine the influence of the height over which eddy viscosity decreases in the near-bed region upon tidal elevations and current profiles, β was reduced from 0.5 (calc 4a) to a value of 0.1 (calc 4b) with k and μ_0 constant (Table 1). Results from this series of calculations showed that even with a factor of 5 change in this parameter, computed M_2 tidal elevation amplitudes only decreased by, on average, the order of 2 to 3 cm with phases changing by the order of a degree (Table 2). Although with a value of $\beta = 0.1$, the rms error and H_s error in the M_2 tide were reduced with H_s changing for M_2 from $H_s = 531$ (calc 4a) to $H_s = 456$ cm (calc 4b) and for M_4 from $H_s = 261$ to $H_s = 253$ cm.

Comparing observed and computed ellipse parameters (calc 4b, Table 4), it is evident that at positions 3, 4, and 5 the near-surface ($\sigma = 0.38$) semimajor axis has increased slightly compared to calculation 2, although close to the bed ($\sigma = 0.92$) it has decreased, giving near-perfect agreement with observations. This change is comparable to that found with calculation 4a. Also, the semimajor axis orientations are in good agreement with the observations. Similarly at positions 6 and 7, the near-bed ($\sigma = 0.88$) semimajor axis is significantly reduced below that given in calculation 2 with a slight reduction below that given in calculation 4a. At positions 16, 17 the near-bed semimajor axis is 2 cm s^{-1} lower than in calculation 2, in good agreement with observations. Again the near-bed current, although not that in the upper part of the water column, is reduced from that found in calculation 4a.

At locations 44, 45, and 46 the near-bed currents are significantly reduced below those found in calculation 2 and are in general below those found in calculation 4a. A similar reduction in near-bed currents is evident at locations 50 to 61. Besides improving the agreement in near-bed currents by reducing β from 0.5 to 0.1, the average deviation in the semimajor axis of the tidal current ellipse decreases from 14% (calc 2) to 10% (calc 4b), with the bias in the histogram of currents (Table 3b) being slightly reduced although currents are still overpredicted.

The improvement in the semimajor axis of the near-bed tidal current ellipse is reflected in the u and v components of current, compare calculations 2 and 4b in Table 5, which clearly shows a reduction in near-bed currents and increase in near-bed shear as viscosity is reduced and bottom friction is increased.

The comparison of results from calculations 2, 4a, and 4b shows that reducing eddy viscosity in the near-bed region with an increase in k leads to a significant improvement in the computed bed currents compared to those found with a constant value of eddy viscosity. Currents in the near-bed layer although not in the upper part of the water column, in general, decrease as β is reduced from 0.5 to 0.1, reflecting an increase in eddy viscosity in the lower part of the water column, with values computed with $\beta = 0.1$, in general, in slightly better agreement with observations.

TABLE 5a. Comparison of observed and computed amplitude U_h (cm s^{-1}) and phase U_g (degrees) of the U component of the M_2 tidal current, at a number of depths and locations.

	Obs		Calc 2		Calc 4b		Calc 5b			
Rig	U_{oh}	U_{og}	U_{ch}	U_{cg}	U_{ch}	U_{cg}	U_{ch}	U_{cg}	h (m)	σ
2	109	228	123	223	123	225	124	226	52	0.30
3	96	222	99	231	102	233	105	234	48	0.38
4	90	222	98	231	99	233	101	234		0.44
5	60	217	73	225	60	225	51	225		0.92
6	85	256	90	231	92	234	95	235	53	0.42
7	66	253	70	226	61	226	55	226		0.88
12	24	267	29	229	28	230	28	231	30	0.56
13	20	264	25	224	23	222	22	221		0.82
15	30	232	31	238	29	237	28	236	23	0.78
16	35	240	37	232	38	236	40	238	22	0.40
17	29	236	32	227	30	228	29	229		0.78
23	42	220	45	221	43	225	42	228	20	0.60
33	75	247	87	240	90	242	93	242	60	0.36
37	40	234	60	227	45	227	32	227	47	0.98
44	74	237	83	232	83	233	84	233	46	0.48
45	72	237	78	230	76	231	75	231		0.62
46	66	236	70	228	65	227	62	227		0.80
50	89	235	98	232	101	233	103	233	57	0.40
51	64	233	77	227	68	225	62	225		0.86
56	78	235	86	229	86	230	87	230	46	0.50
60	57	226	62	224	61	224	60	224	28	0.50
61	46	218	49	218	45	217	42	216	20	0.76

To examine in more detail the effect of changing viscosity in the near-bed region while maintaining k and β fixed, a calculation was performed with near-bed eddy viscosity reduced to μ_1:μ_0 is 1:0.04 (calc 5a, Table 1).

It is evident from Tables 2 and 3a (compare calcs 5a and 4b) that this change in viscosity, on average, changes M_2 tidal elevations and phases by less than 1 cm or 1 deg, with the error histogram showing an in-

TABLE 5b. Comparison of observed and computed amplitude V_h (cm s^{-1}) and phase V_g (degrees) of the V components of the M_2 tidal current, at a number of depths and locations.

	Obs		Calc 2		Calc 4b		Calc 5b			
Rig	V_{oh}	V_{og}	V_{ch}	V_{cg}	V_{ch}	V_{cg}	V_{ch}	V_{cg}	h (m)	σ
2	17	228	27	229	25	232	25	235	52	0.30
3	13	235	21	252	22	254	23	255	48	0.38
4	17	237	22	252	22	255	23	256		0.44
5	19	255	20	257	18	258	16	259		0.92
6	13	50	12	291	12	292	12	293	53	0.42
7	8	25	14	288	14	287	13	286		0.88
12	25	320	21	264	19	268	18	269	30	0.56
13	26	322	19	263	17	265	15	266		0.82
15	25	269	25	279	22	281	20	281	23	0.78
16	23	340	23	316	21	319	20	321	22	0.40
17	19	334	21	310	18	310	17	310		0.78
23	29	1	21	357	18	5	17	10	20	0.60
33	25	247	35	247	35	247	35	248	60	0.36
37	4	248	10	247	8	251	6	253	47	0.98
44	6	221	8	219	7	215	6	215	46	0.48
45	4	218	8	230	7	232	6	234		0.62
46	7	230	8	241	8	247	7	250		0.80
50	12	207	10	201	10	204	10	206	57	0.40
51	10	215	9	234	10	243	10	245		0.86
56	5	68	7	79	8	77	9	75	46	0.50
60	10	50	12	36	12	37	13	37	28	0.50
61	12	21	12	18	11	19	10	18	20	0.76

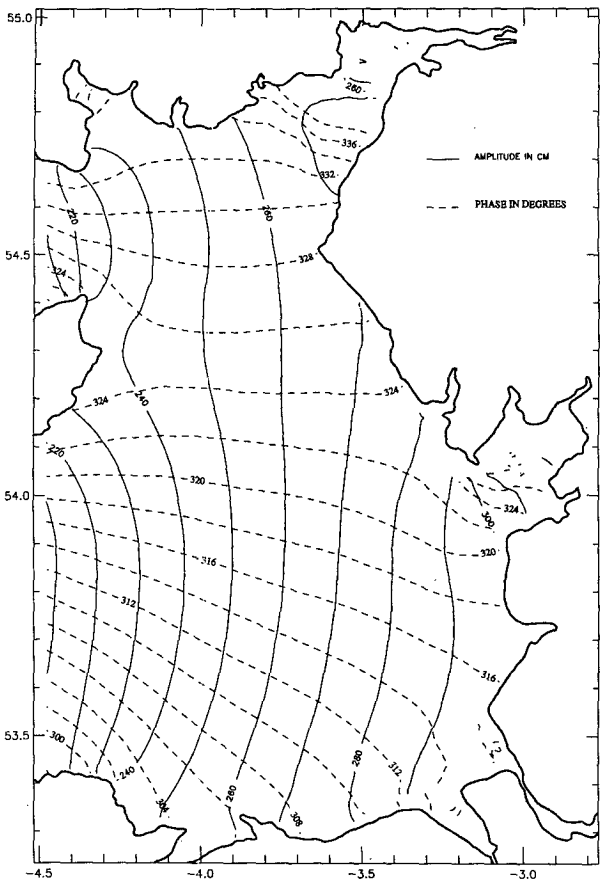

FIG. 4. Computed M_2 cotidal chart determined with the full three-dimensional model (calc 4b in Table 1).

creased bias to overestimate elevations. The number of points at which computed exceeds observed by 5 cm increases from 6 to 10, with an increase in H_s from 456 to 468 cm. This reduction in elevation damping is to be expected as bottom viscosity is decreased with k fixed.

Comparing tidal current ellipse parameters (calcs 5a and 4b in Table 4) it is evident that the change in bed viscosity has no influence upon currents in the upper part of the water column, although at location 5 (σ = 0.92) the near-bed current increases from 61 to 64 cm s^{-1} as bed viscosity is reduced with a similar change at locations 7 (σ = 0.88) and 51 (σ = 0.86) between calculations 4b and 5a. No significant changes in orientation with this reduction in viscosity were evident.

From the histogram of current ellipse parameters (Table 3b) it is evident that in calculation 5a the bias to overestimate currents has increased compared to that found in calculation 4b. This increase is to be expected since, as shown in Table 4, reducing the near-bed viscosity leads to an increase in currents in the lower part of the water column.

To examine the influence of the bottom friction coefficient the $\mu_1:\mu_0$ ratio was fixed at 1:0.04, with β = 0.1 and k increased from k = 0.01125 (calc 5a) to k = 0.03375 (calc 5b, Table 1). This increase in bottom friction coefficient reduced M_2 tidal elevation amplitudes in shallow water by the order of 2 cm with phase changes of the order of 2 deg (Table 2, compare calcs 5a and 5b). From the histogram of M_2 tidal elevation errors, there is a bias in the model to underpredict elevations (compare 5a and 5b in Table 3a) with H_s increasing from 468 to 486 cm. As expected, increasing k increases the damping in the solution.

Comparing tidal ellipse parameters (calc 5b, Table 4) it is evident that shear in the near-bed region has been increased due to a small increase in surface currents, with near-bed currents having decreased significantly below those found in calculation 4b and, in general, below observed values.

The rms error in the computed semimajor axis has been reduced to 10.3 cm s^{-1} together with a reduction in the bias in the histogram of errors. However, that the model with these parameter settings underestimates computed elevations (Table 3a) and near-bed currents does suggest that there is excessive damping in the model.

d. *Comparison of spatial distributions*

To understand the influence of bed viscosity and bottom friction upon tidal currents, it is interesting to examine the spatial distribution of tidal current ellipses and bed stress distributions computed in calculations (4b) and (2), where different viscosity profiles were used.

The computed M_2 cotidal chart (Fig. 4) determined in calculation 4b with reduced viscosity in the near-bed region, but K = 0.01125 is not significantly different from that determined with the hybrid three-dimensional model (calc 1) or constant viscosity model with K = 0.00375 (calc 2). Spatial distributions of the major and minor axes of the M_2 tidal current ellipse at the sea surface and seabed (Figs. 5a,b) show strong rectilinear tidal currents near the open boundary of the model with tidal current magnitude decreasing rapidly with distance from this boundary. A region of more circular tidal current ellipses with significantly reduced magnitude is clearly evident to the east of the Isle of Man. The M_2 tidal current ellipse distribution at the seabed (Fig. 5b) shows a similar spatial distribution to that found for the surface currents, although current magnitude is much smaller.

Contours of the time-averaged eddy viscosity over a tidal cycle (Fig. 6a), and maximum viscosity (Fig. 6b) computed using Eq. (9), clearly show that viscosity is a maximum in the region of open boundaries where water depths and tidal currents (Figs. 5a,b) are a maximum. In the region of the open boundary the time-averaged viscosity exceeds 0.08 m^2 s^{-1} (800 cm^2 s^{-1})

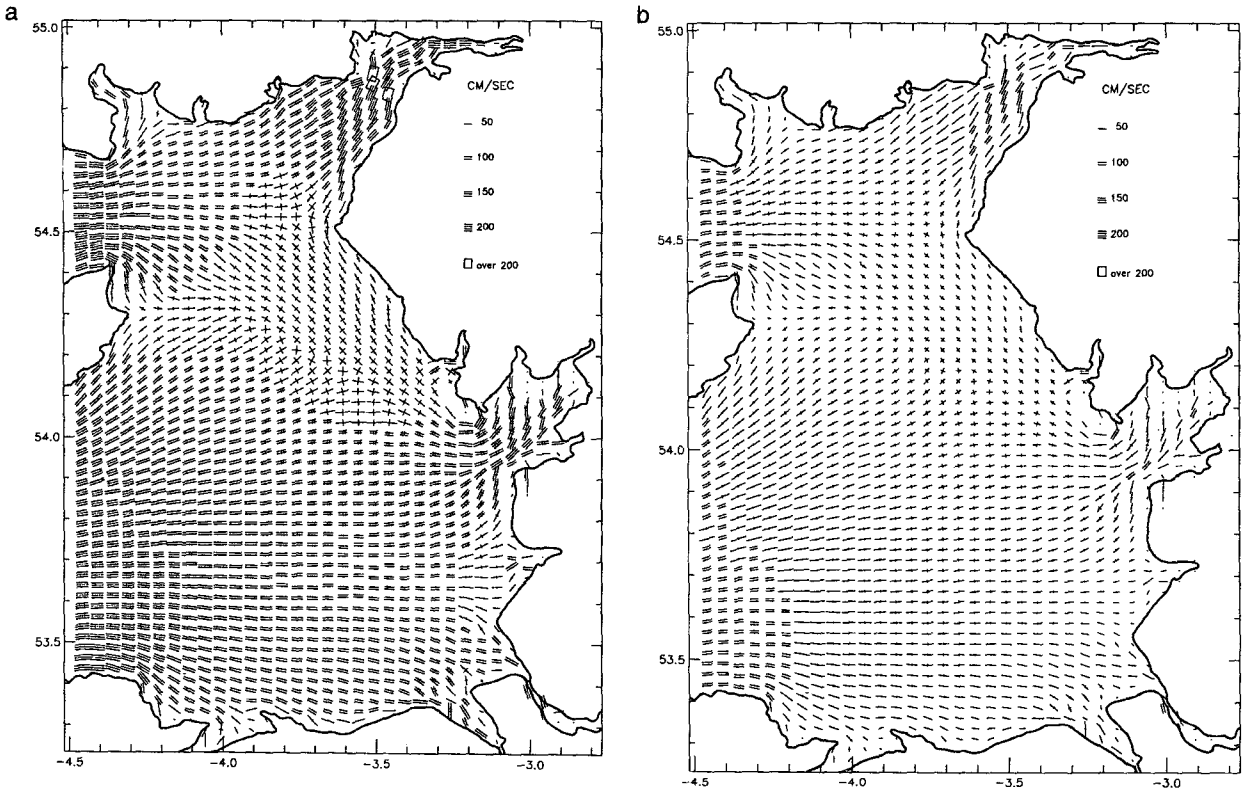

FIG. 5. Computed M_2 tidal current ellipses (a) sea surface and (b) sea bed determined with the full three-dimensional model (calc 4b in Table 1).

with maximum values exceeding 0.12 $m^2 s^{-1}$. In shallow nearshore regions where tidal velocities are lower, the time-averaged viscosity is below 0.01 $m^2 s^{-1}$ with a similar reduction in the maximum eddy viscosity.

Contours of the maximum bed stress determined in calculation 4b (Fig. 7a) show a region of high stress (exceeding 2 N m^{-2}) close to the open boundaries where tidal current velocities are large with smaller bed stresses in the interior, particularly in the region off the west coast of Cumbria. The reduced bed stress off the Cumbrian coast partially explains the existence of the mud patch in this region [see Aldridge and Davies (1993) for details of regional bed types in the area].

Tidal current ellipse distributions computed in calculation 2 (eddy viscosity profile A and $K = 0.00375$) at the sea surface were not significantly different from those determined in calculation 4b, although maximum bed currents were larger. Also maximum and time-averaged eddy viscosity distributions and magnitudes were not significantly different from those determined in calculation 4b, suggesting that above the bottom boundary layer viscous effects were similar and that the differences in the computed current profiles in calculations 2 and 4b arise from the reduction in near-bed viscosity in run 4b and changes in bed stress.

Although the M_2 cotidal charts and current ellipses in the upper parts of the water column computed in calculation 2 (viscosity profile A, $K = 0.00375$) and calculation 4b (viscosity profile B, $K = 0.01125$) and bed stress distribution show similar patterns (compare Figs. 7a and 7b), it is evident that the magnitude of the bed stress in calculation 2 is of order 0.25 N m^{-2} lower than in calculation 4 (in some areas a difference of the order of 25%) compared with differences of the order of only 2% in surface elevations or tidal current magnitudes in the upper part of the water column.

These differences in maximum bed stress (although surface elevations and currents between the two formulations of the bottom boundary layer are similar) clearly show how important it is to ensure the correct frictional level in the bottom boundary layer and compare near-bed currents with observations if a tidal model is to be used to determine bed stress values. Obviously a comparison with surface elevations or currents in the upper part of the water column is not sufficient to ensure that the model is correctly determining quantities such as the bed stress, which are important in sediment transport problems.

e. Comparison of overtides

Since the model contains all the nonlinear terms (namely, advection, wave drift, quadratic friction, and time-dependent viscosity) necessary to determine the

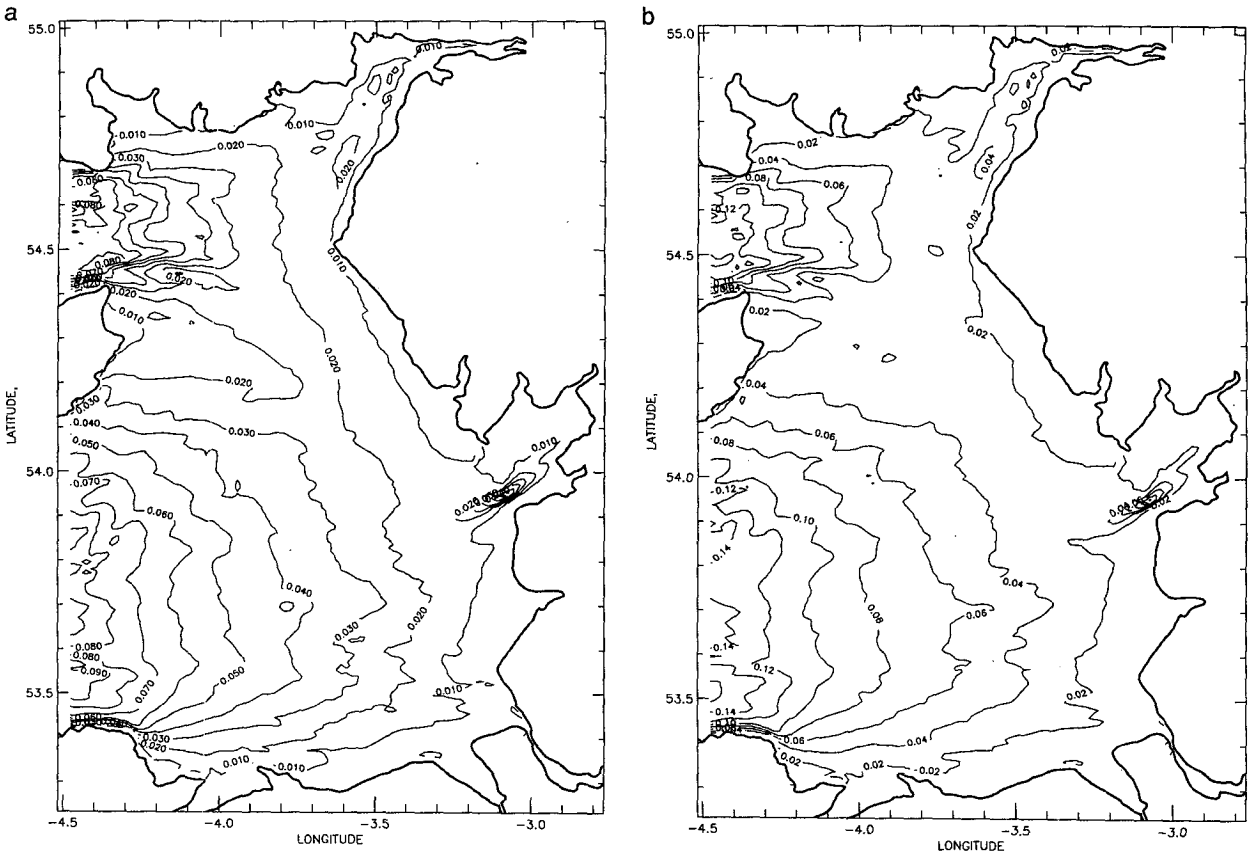

FIG. 6. Contours of (a) time-averaged and (b) maximum viscosity ($m^2 s^{-1}$) over a tidal cycle computed using the three-dimensional model (calc 4b in Table 1).

higher harmonics and has a sufficiently fine grid to resolve these harmonics, it is interesting to consider any differences in these harmonics between calculations 2 and 4b due to frictional effects.

The M_4 cotidal chart determined in calculation 4b (Fig. 8) shows the M_4 tidal amplitude increasing significantly in shallow water regions, in particular in the Solway, with tidal phase increasing from west to east and south to north. A comparison at offshore and shore-based gauges (Table 6) shows that at certain gauges in the Liverpool Bay region, namely, locations (b), (e), (o), (r), and (u), the model can accurately reproduce the amplitude of the M_4 tide although in other shallow water regions, for example, Morecambe, the model overestimates the M_4 tide probably because drying occurs in this area giving rise to a discontinuous time series that when analyzed gives a spuriously larger higher harmonic.

Repeating the calculation, (calc 4L) but omitting the advective terms, leads to a slight reduction of the M_4 tidal amplitude in the nearshore region, although the change is small. The reason for this is that the rapid increase in the M_4 tidal amplitude in the shallow regions of the eastern Irish Sea has been shown, using a coarse grid model of the whole Irish Sea (Davies and Lawrence 1994), to be due to the wave drift term; namely, the retention of the $(h + \zeta)$ term in the equations, rather than the nonlinear advective terms. (Details of the relative importance of the various terms is given in Davies and Lawrence 1994.)

Spatial distributions of surface and bed M_4 tidal current ellipses (Figs. 9a,b) show strong M_4 currents in shallow water regions such as the Solway and Morecambe Bay. However, off the coast of Cumbria the M_4 tidal currents are much weaker with slightly stronger tidal currents in the southern part of the region. In general, M_4 tidal currents are an order of magnitude smaller than the M_2 currents, with bed currents significantly smaller than surface currents due to the influence of bottom friction.

Initially considering calculation 4b in Table 7, at locations 3, 4, and 5, the semimajor axis is in good agreement with observations, with frictional effects decreasing the M_4 currents in the near-bed region. Similar good agreement is evident at positions 6 and 7. At positions 12 and 13 to the east of the Isle of Man the computed semimajor axis is less than the observed, the reason for which is not clear.

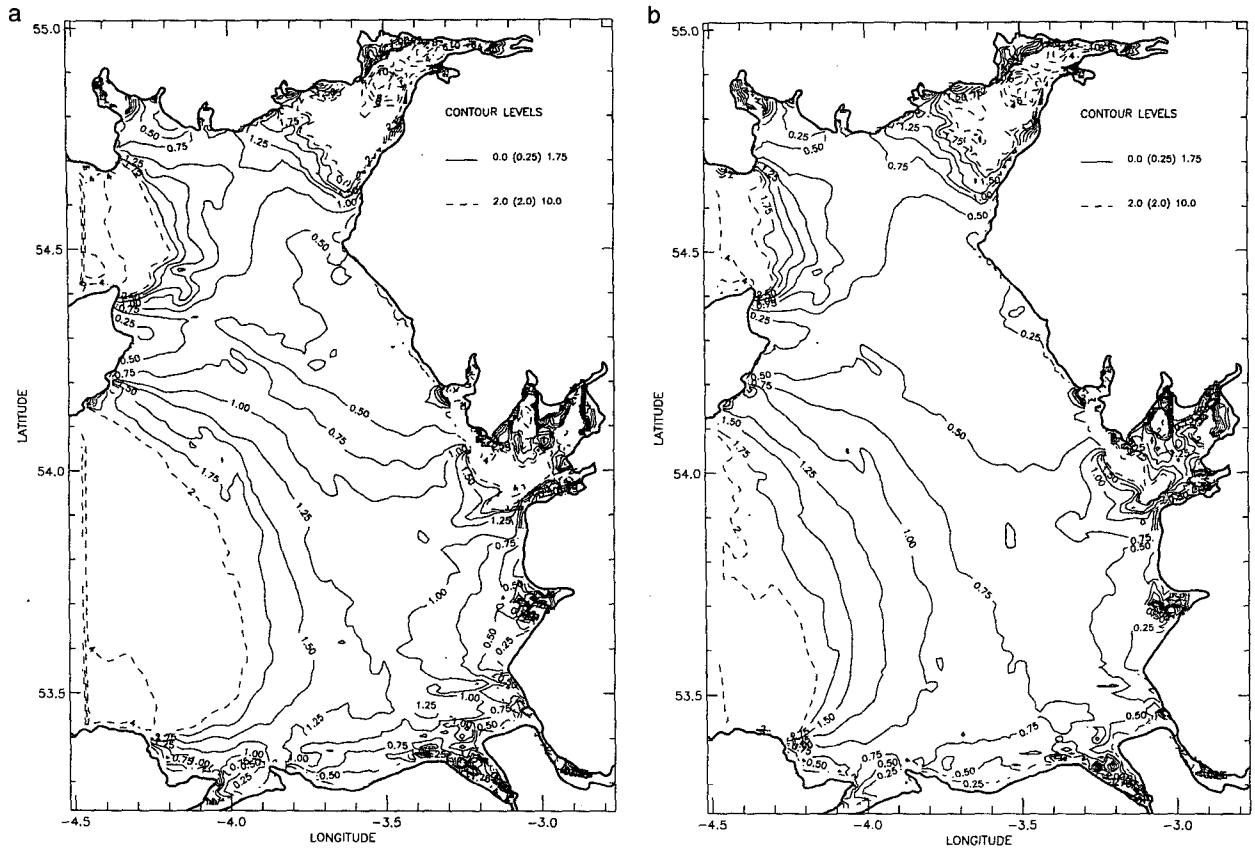

FIG. 7. Contours of maximum bed stress (N m^{-2}) over a tidal cycle determined using the three-dimensional model, (a) calc 4b and (b) calc 2 in Table 1.

At shallow water locations in Morecambe Bay, for example, position 18, the strong (of order 20 cm s^{-1}) M_4 tidal current is reproduced by the model, which also reproduces the significant reduction just south of this location at position 32 and to the east at location 23. The ability of the model to resolve the rapid change in M_4 tidal current between locations 18 and 32 is, of course, only possible because of the high-resolution grid used in the model.

At deeper water positions, namely, 37, 44, 45, and 46, the intensity of the M_4 tide together with its reduction in the near-bed layer at location 37 is reproduced with the model together with the orientation of the tidal current ellipse; similar good agreement is evident at positions 50 and 51. At nearshore locations in Liverpool Bay and along the Welsh coast, namely, positions 58, 59, 60, and 61, the model can accurately reproduce current magnitude although, on average, the direction of the ellipse is in error by the order of 10°.

The histogram of errors shows that there is a slight bias in the model to overpredict M_4 tidal currents with the major axis being reproduced with an rms error of 2.1 cm s^{-1} and the orientation to within 4.7°. These results are particularly good considering that there can be a significant error in the M_4 tidal currents derived from a month of observations (Pugh and Vassie 1976).

The tidal current ellipse parameters computed without the advective terms but for viscosity varying in the vertical (run 4L) and constant eddy viscosity through the vertical (run 2L) show that, on average, the computed M_4 tidal currents are lower than those found in run 4b (compare results in Table 7). Also, shear in the vertical in calculation 2L is less than in calculation 4L.

The computed M_6 cotidal chart revealed a high degree of spatial variability in the M_6 tidal amplitudes, which increase rapidly in very shallow regions from the order of 1 cm to 7 cm. The phase of the M_6 also changes rapidly over quite short distances, with an amphidromic point to the west of Morecambe Bay connected to a second point to the northeast of this location.

Surface and bed M_6 tidal current ellipse distributions showed very small currents of order 2 cm s^{-1} in offshore regions with a rapid increase in nearshore shallow water areas of up to 20 cm s^{-1}. A reduction in current magnitude due to frictional effects was evident close to the seabed.

Comparing observed and computed M_6 tidal elevations (Table 8), and current ellipses (Table 9) with and without the advective terms, it is evident that these terms do not have a significant effect upon the M_6 tide. Also, despite the fine resolution of the model's grid, there are some significant errors, with the model tending to overpredict the M_6 tidal elevation and currents. Since the M_6 tide has a very small magnitude, there may be some significant errors in the observed values (Pugh and Vassie 1976). However, despite possible errors in the observations, there does appear to be a bias in the computed results. Frictional effects are known to have an influence upon the M_6 tide and that the present model, unlike the earlier model of Davies and Jones (1992), does not contain the S_2, N_2, O_1, K_1 tidal constituents may have some influence. (The results of the M_6 comparison are inconclusive since these additional constituents are omitted and calculations using a larger number of constituents would be required to determine the correct frictional level.)

f. Tidal residuals

The nonlinear terms in the three-dimensional hydrodynamic equations, besides generating the higher harmonics, are also responsible for producing a tidal residual. In an initial series of calculations, the advective terms were omitted although the other nonlinear terms were retained, and eddy viscosity was held constant in the vertical with $K = 0.00375$ (in essence, calc 2 without advection, which we will denote as calc 2L, in Table 1).

Surface tidal residuals (Fig. 10a) show a strong northward flow along the Cumbrian coast, of order 10 cm s^{-1}, with a residual flow out of the Solway. The residual flow in Morecambe Bay is, in essence, a residual outflow along the northern and southern edges of the basin with an inflow in the center of the region. In offshore regions the residual flow is much weaker, with a fairly uniform eastward flow in the southern part of the region and a more spatially varying residual in the northern part of the area, reflecting the decrease in tidal current between the area to the north and east of the Isle of Man.

Tidal residuals at the seabed (Fig. 10b) in shallow water regions exhibit similar spatial distribution compared to those at the sea surface, although in offshore regions, particularly in the southern part of the model, the tidal residual exhibits more spatial variability.

Surface tidal residuals computed using the varying viscosity profile with $K = 0.01125$, again with the omission of advection (calc 4L), were not significantly different from those determined previously, although at the seabed (Fig. 10c) a more uniform residual flow is evident. In both these calculations the tidal residual elevation in offshore regions was negligible, although within the Solway residual elevations increased from below 1 cm to over 10 cm in the very shallow water.

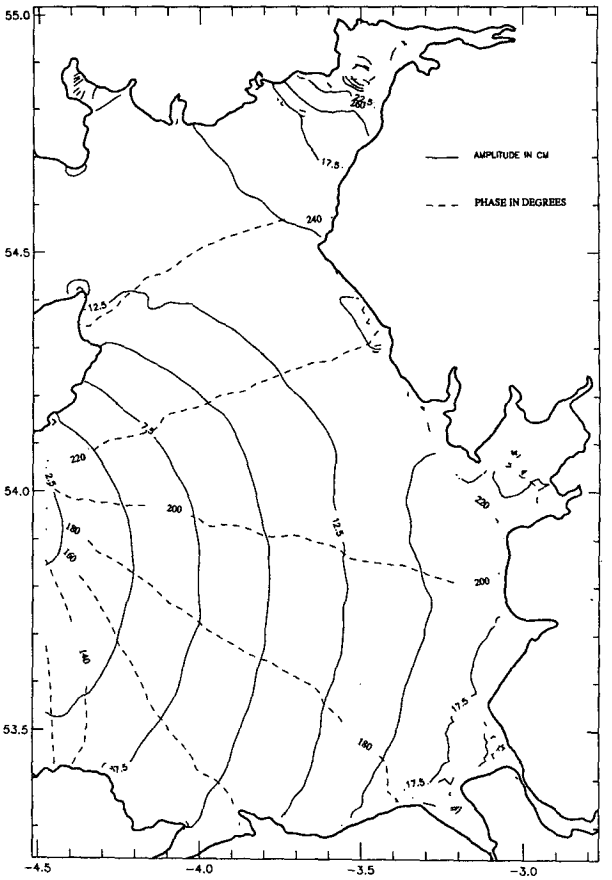

FIG. 8. Computed M_4 cotidal chart determined with the full three-dimensional model (calc 4b in Table 1).

Repeating calculation 4L, but with the advective terms included (calc 4b), produced a significant increase in tidal residual elevations (Fig. 11a) and flows (Figs. 11b,c) in offshore regions, with residual elevations in some deep water areas of the order of 2 cm (Fig. 11a).

Surface residual currents (Fig. 11b) with the inclusion of the advective terms show significantly more spatial variability than the solution without advection (Fig. 10a). However, in the shallow coastal regions where the residual flow is strongest both solutions are similar, although the advective terms do introduce some finer-scale features. One significant difference between the two solutions is the region of strong residual flow that occurs northeast of the Isle of Man when the advective terms are included (Fig. 11b) but is not found when these terms are omitted (Fig. 10a). In this region tidal currents are strong and change direction quite rapidly (Fig. 5); hence the nonlinear terms are large and make a significant contribution to the tidal residual.

The tidal residual surface currents computed with the model, using viscosity varying in the vertical, show

TABLE 6. Comparison of errors $\Delta\zeta$ (cm) in amplitude and Δg (deg) in phase for M_4 tidal amplitude ζ (cm) and phase g (deg).

		Obs		Calc 4b		Calc 4L	
Point	Port	ζ_0	g_0	$\Delta\zeta$	Δg	$\Delta\zeta$	Δg
a	Barrow	19	252	6	−13	3	−17
b	Birkenhead	23	217	−2	−46	−0	−42
c	Douglas	5	233	−0	−2	−1	−2
d	Heysham	19	243	−5	7	−6	17
e	Hilbre	19	203	1	−19	−0	−19
f	Liverpool	23	213	−1	−45	−2	−41
g	Formby	25	235	−6	−48	−9	−44
h	Hestan	11	280	4	−22	5	−22
i	Liverpool Bay	21	196	−4	−11	−6	−11
j	Ramsay	7	237	3	1	3	4
k	Workington	13	253	3	−3	5	−5
l	Wylfa Head	4	182	1	−73	3	−82
m	Liverpool	21	201	3	−25	0	−24
n	Llandudno	12	181	−0	−15	−1	−20
o	New Brighton	23	198	3	−21	−1	−19
p	Amlwch	6	185	−0	−40	1	−61
q	Ost G	17	196	0	−11	−1	−10
r	Queens channel	16	197	0	−12	−0	−11
s	STD Irish Sea	6	200	−0	−22	−0	−31
t	Stn10	16	199	−5	−9	−6	−9
u	Stn34	11	216	0	−2	0	3
v	Stn35	11	247	3	−1	4	0
w	Creetown	30	274	1	−17	1	−16
x	Conwy	26	216	−14	−55	−15	−56
y	Barrow RI	30	274	−9	−39	−11	−39
z	Barrow HP	26	216	−5	22	−7	18
aa	Barrow HS	16	199	0	23	−2	20
bb	Morecambe	11	216	20	42	19	47
cc	Fleetwood	11	247	5	−17	4	−14

TABLE 7. Comparison of observed and computed semimajor axis A (cm s^{-1}), orientation T (deg), and rotation R of the M_4 tidal current ellipse at a number of depths and locations.

	Obs			Calc 4b			Calc 4L			Calc 2L				
Rig	A_0	T_0	R_0	A_c	T_c	R_c	A_c	T_c	R_c	A_c	T_c	R_c	h (m)	σ
3	4.9	34	−	4.7	18	+	4.4	27	−	3.0	36	+	48	0.38
4	4.5	18	+	4.6	18	+	4.3	26	−	3.0	35	+		0.44
5	3.8	139	+	3.0	20	+	2.8	24	+	2.4	32	+		0.92
6	4.2	20	−	4.2	47	−	3.6	23	+	2.5	36	+	53	0.42
7	2.9	163	+	2.9	45	−	2.6	201	+	2.1	211	+		0.88
12	10.7	41	−	6.4	61	+	7.3	65	+	7.1	69	+	30	0.56
13	10.9	40	−	5.5	60	+	6.1	63	+	6.3	67	+		0.82
18	21.8	64	+	25.6	71	+	22.3	74	+	21.5	71	+	3	0.24
23	4.5	7	+	4.0	20	+	3.5	28	+	3.6	37	+	20	0.60
24	9.7	52	+	18.0	46	+	18.4	42	+	18.0	43	+	7	0.20
32	11.9	54	−	13.8	30	+	12.2	29	+	12.8	30	+	11	0.40
33	6.3	29	−	7.2	10	+	7.5	29	+	6.4	30	+	60	0.36
37	2.5	10	+	3.9	10	+	3.7	13	+	4.4	11	+	47	0.98
44	5.8	10	−	6.5	10	+	6.2	13	+	5.5	11	+	46	0.48
45	5.7	15	−	6.2	10	+	5.9	12	+	5.3	10	+		0.62
46	5.4	11	−	5.5	9	+	5.2	12	+	5.0	10	+		0.80
50	6.9	19	−	6.7	6	+	6.6	12	+	5.6	11	+	57	0.40
51	5.3	5	−	5.0	4	+	4.9	11	+	4.9	8	+		0.86
56	5.9	189	−	7.2	1	+	6.3	179	+	5.7	178	+	46	0.50
57	5.1	165	+	5.7	178	+	5.0	181	+	4.3	181	+	33	0.22
58	3.4	172	+	6.2	157	+	4.3	150	+	4.0	148	+	16	0.52
59	4.5	180	+	5.0	166	+	4.3	164	+	4.3	160	+	20	0.62
60	5.4	171	+	5.2	175	+	4.6	173	+	4.3	172	+	28	0.50
61	4.7	186	+	3.8	165	+	3.7	170	+	3.7	167	+	20	0.76

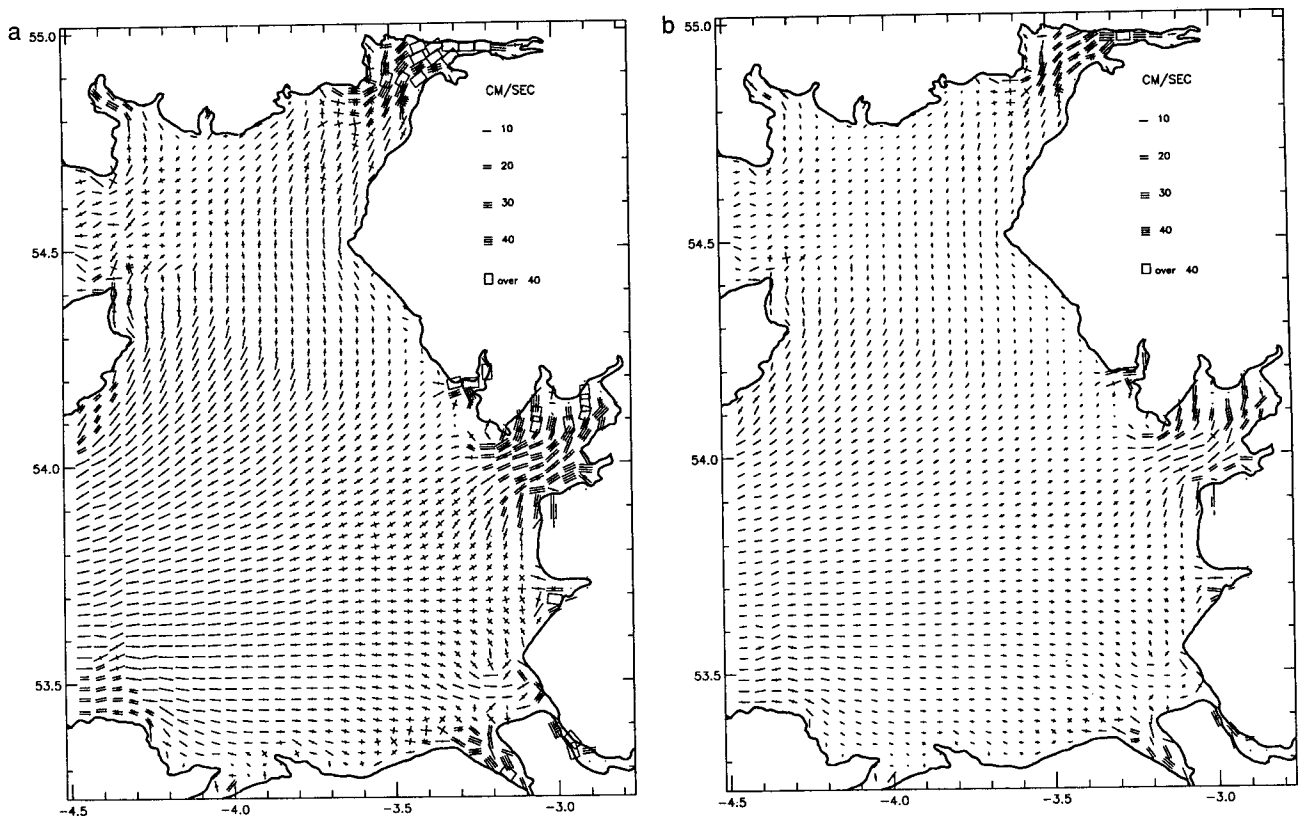

FIG. 9. Computed M_4 tidal current ellipses (a) sea surface and (b) seabed determined with the three-dimensional model (calc 4b in Table 1).

similar spatial distributions to the depth-mean residuals shown in Aldridge and Davies (1993), determined with a two-dimensional model. This similarity suggests that a tidal residual computed from a two-dimensional model may be a reasonable representation of residual flow in the upper part of the water column. However, tidal residual currents at the seabed (Fig. 11c) in offshore areas show significantly less spatial variability than those in the upper part of the water column. Also, due to frictional effects the magnitude of the near-bed residual currents is smaller than those in the upper part of the water column. Also, near-bed residual currents, like tidal currents, are influenced by the near-bed frictional effects, with smaller computed currents in calculation 4b than in 2.

The differences between depth-mean and near-bed tidal residuals and the influence of bottom friction upon them is important in determining the long-term residual transport of material such as sediments, which is influenced more by the near-bed than near-surface residual flows.

5. Concluding remarks

The three-dimensional high-resolution eastern Irish Sea model, applied previously by Aldridge and Davies (1993) to examine the M_2 tide in the region, has been used here to investigate the spatial distribution of higher harmonics.

Initially, the model was formulated in such a fashion that the bed stress was computed from the depth mean current, giving a hybrid two-dimensional/three-dimensional model. By this means the model computes identical surface elevations and depth-mean currents as a conventional two-dimensional model but with the additional feature of determining the tidal current profile. Although not rigorously physically correct, in that the bed stress should be computed from the near-bed current, this approach is useful in that changes in current profile due to viscous effects can be separated from those due to changes in bottom stress. (When bottom stress is determined from bottom currents, then changes in viscosity influence both the current profile and the bed stress, which in turn affects the current.)

Initial calculations using this model with eddy viscosity constant in the vertical, although varying in time, showed that it could reproduce tidal elevations although tidal currents in the bottom boundary layer were overestimated. Retaining this eddy viscosity formulation but determining the bed stress in terms of the bed current with a friction coefficient twice as large as that used in the hybrid model yielded similar (although slightly improved) elevation distributions, although near-bed currents were overestimated. This overesti-

TABLE 8. Comparison of errors $\Delta\zeta$ (cm) in amplitude and Δg (deg) in phase for M_6 tidal amplitude ζ (cm) and phase g (deg).

		Obs		Calc 4b		Calc 4L	
Point	Port	ζ_0	g_0	$\Delta\zeta$	Δg	$\Delta\zeta$	Δg
a	Barrow (Furness)	3	49	5	−109	5	−112
b	Birkenhead	5	320	3	−68	4	−64
c	Douglas	1	354	1	65	1	59
d	Heysham	2	10	8	−93	7	−96
e	Hilbre Island	2	32	1	−173	1	−172
f	Liverpool	5	322	3	−62	5	−57
g	Formby	5	11	−2	−149	−2	−147
h	Workington	2	324	1	176	1	176
i	Liverpool (GD)	5	349	3	−87	3	−93
j	Llandudno	2	355	−1	−160	−1	−153
k	New Brighton	5	329	2	−64	2	−67
l	Ost G	4	13	−1	−151	−0	−147
m	Queens Channel	3	17	0	−154	0	−149
n	STD Irish Sea	1	354	0	11	1	10
o	Stn10	3	335	−2	−79	−2	−77
p	Stn34	1	6	−1	167	−1	−162
q	Stn35	1	234	2	−107	2	−106
r	Creetown	5	117	7	25	7	24
s	Conwy	6	21	−4	53	−5	66
t	Barrow RI	5	117	1	−172	1	−178
u	Barrow HP	6	21	1	−79	1	−77
v	Barrow HS	3	335	2	−66	1	−61
w	Morecambe	1	6	5	16	4	7
x	Fleetwood	1	234	5	38	5	37

TABLE 9. Comparison of observed and computed semimajor axis A (cm s^{-1}), orientation T (deg), and rotation R of the M_6 tidal current ellipse at a number of depths and locations.

	Obs			Calc 4b			Calc 4L			Calc 2L				
Rig	A_0	T_0	R_0	A_c	T_c	R_c	A_c	T_c	R_c	A_c	T_c	R_c	h (m)	σ
2	3.1	2	+	6.1	117	+	6.2	117	−	6.3	135	+	52	0.30
8	2.4	110	+	3.8	138	+	3.3	152	−	3.5	177	−	54	0.86
9	0.7	146	+	1.2	107	+	1.1	112	+	1.0	130	+	15	0.86
15	1.0	139	+	1.7	127	−	1.5	131	−	1.5	97	−	23	0.78
23	1.1	159	+	4.1	159	+	4.1	156	+	2.7	156	−	22	0.60
24	2.3	64	+	9.5	58	+	9.5	56	+	7.8	58	+	5	0.20
32	1.9	2	−	9.5	47	+	8.6	55	+	6.9	60	+	5	0.40
33	1.3	4	+	1.1	90	+	0.5	100	+	1.5	30	+	56	0.36
34	2.5	161	+	2.5	175	+	2.5	174	+	1.3	170	+	21	0.62
35	1.6	6	+	2.4	0	+	2.4	176	+	1.3	159	−	21	0.40
37	0.8	200	−	2.5	159	+	2.5	158	+	1.8	147	−	42	0.98
38	1.5	173	−	1.2	163	−	1.3	163	−	0.6	102	+	40	0.38
39	1.6	155	+	1.8	155	+	1.9	156	+	0.7	97	−	40	0.60
44	1.2	167	−	1.2	158	+	1.3	159	+	0.9	52	+	42	0.48
45	1.2	166	+	1.9	151	+	1.9	153	+	0.9	83	−	42	0.62
46	0.8	155	−	3.0	151	+	3.0	152	+	1.5	132	−	42	0.80
50	1.6	184	−	1.2	139	+	1.4	124	+	1.9	43	+	59	0.40
51	0.8	23	+	3.1	140	+	3.5	140	+	2.2	114	−	59	0.86
56	1.3	167	+	1.1	160	+	1.2	163	+	0.9	199	+	44	0.50
57	1.8	162	−	0.9	175	−	1.0	176	−	0.7	131	−	27	0.22
58	2.1	152	−	2.5	187	+	2.5	188	+	1.1	200	+	21	0.52
59	1.6	186	+	2.1	175	+	2.3	175	+	0.7	164	+	21	0.62
60	2.0	165	−	1.7	177	+	1.7	180	+	0.3	112	+	22	0.50
61	1.0	174	+	2.3	160	+	2.4	161	+	1.0	144	+	21	0.76

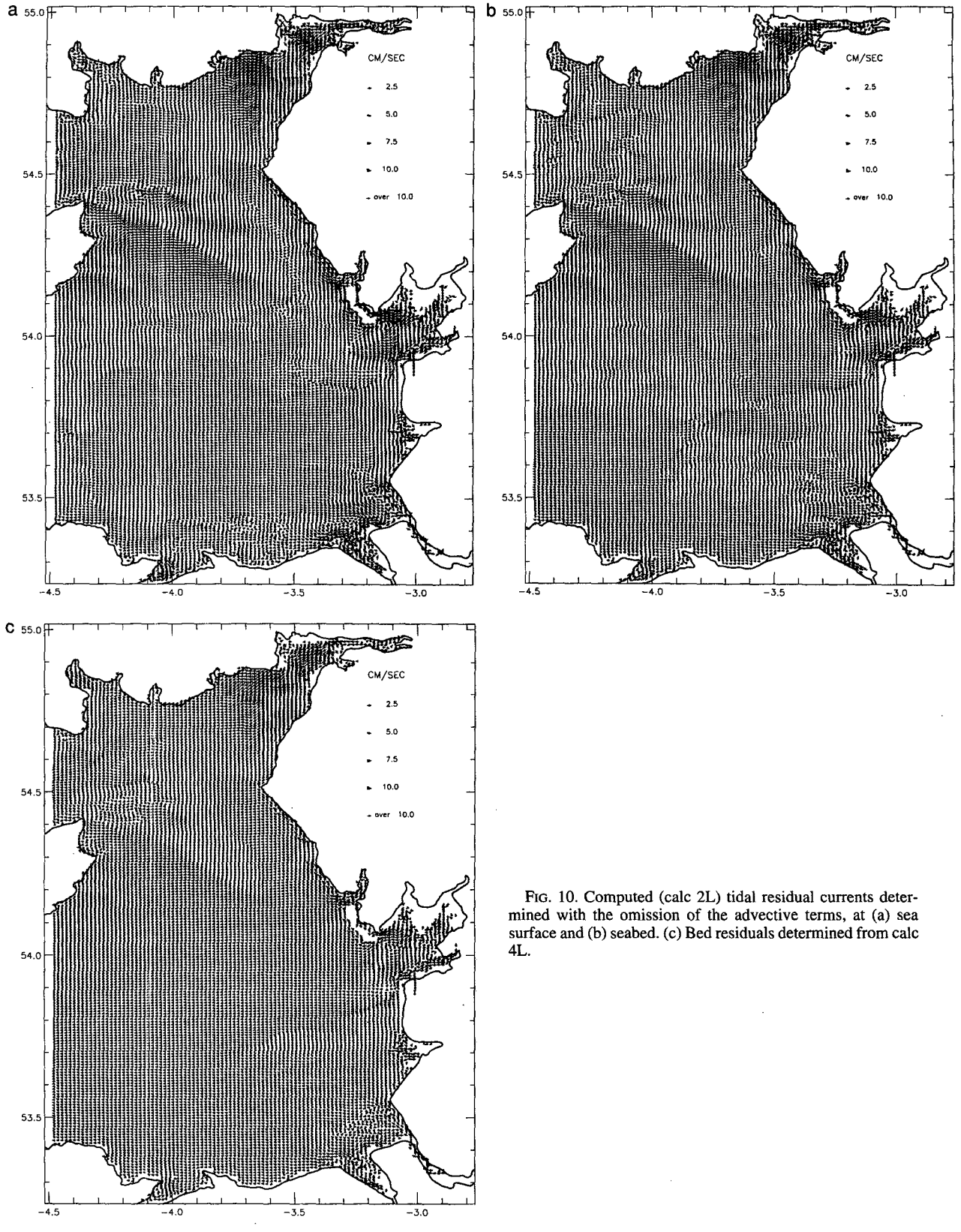

FIG. 10. Computed (calc 2L) tidal residual currents determined with the omission of the advective terms, at (a) sea surface and (b) seabed. (c) Bed residuals determined from calc 4L.

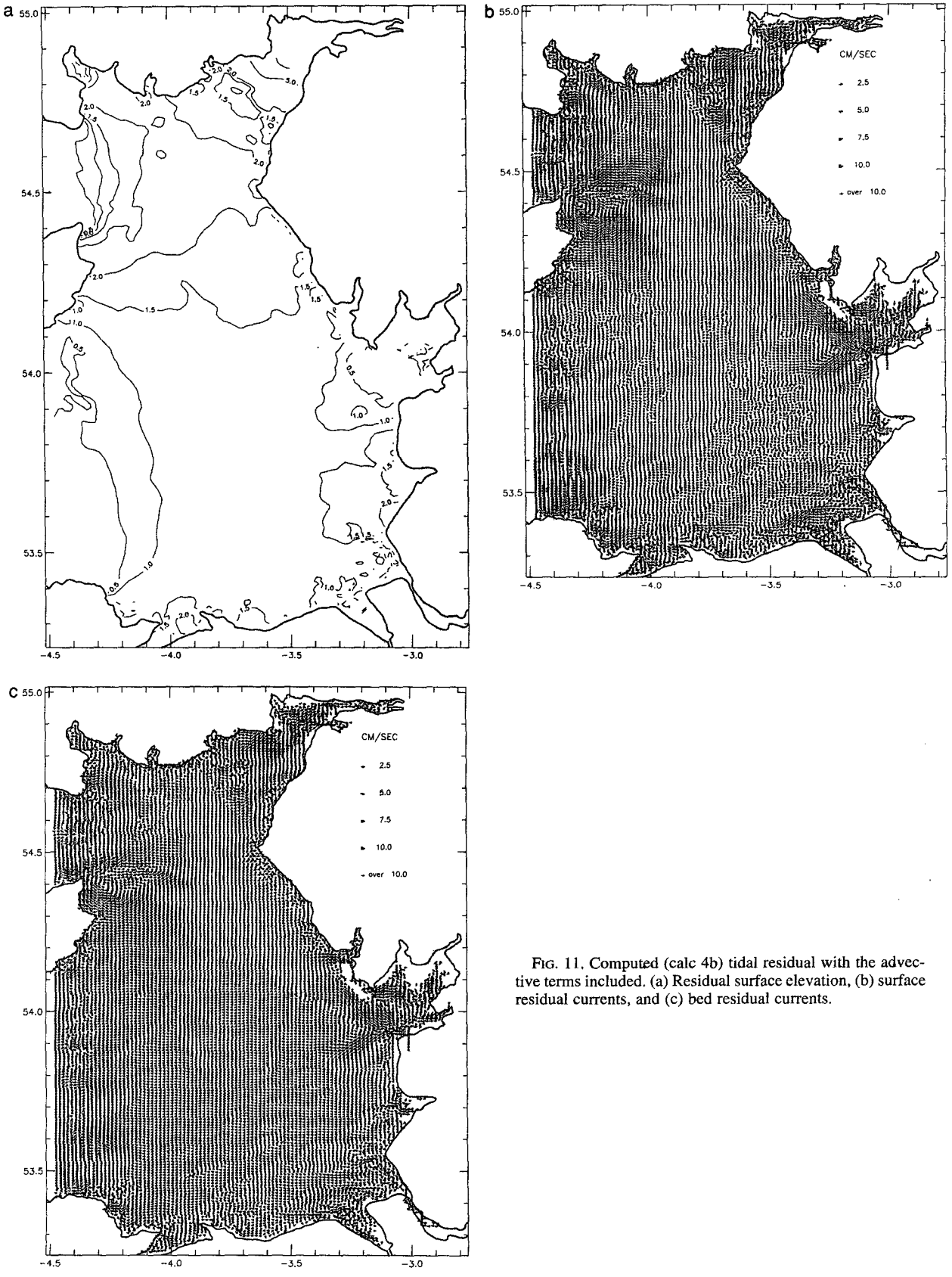

FIG. 11. Computed (calc 4b) tidal residual with the advective terms included. (a) Residual surface elevation, (b) surface residual currents, and (c) bed residual currents.

mation of M_2 bed currents with a constant eddy viscosity in the vertical is similar to that found by Aldridge and Davies (1993) with an identical viscosity profile. Results of the series of calculations aimed at determining the sensitivity of elevations and currents to changes in the thickness of the near-bed region over which eddy viscosity decreases in a linear manner, and the value of bottom viscosity, showed that elevations and currents in the upper part of the water column were insensitive to variations in these parameters. However, a reduction in eddy viscosity in the near-bed region and an increase in bottom friction coefficient by a factor of 3 above that used with a constant viscosity profile yielded a significant improvement in the near-bed currents, which were found to be in good agreement with observations, with little change in tidal elevations.

The current comparisons presented here show that, by using a slip condition with an enhanced bottom drag coefficient and near-bed reduction in viscosity, bed currents of comparable accuracy to those obtained by Davies (1993) using a no-slip condition are obtained. The advantage of the present approach over that of Davies (1993) is that a time-split integration method can be used with an associated significant saving in computer time, especially with a fine horizontal grid in deep water regions.

A comparison of maximum bed stress over a tidal cycle between the two viscosity profiles shows that although elevations and near-surface currents are not particularly sensitive to the near-bed form of the eddy viscosity, the bed stress is particularly sensitive. In problems such as sediment transport where a detailed knowledge of the bed stress is important, it is essential to check that the model can accurately reproduce bed currents. Relying upon reproducing elevations and surface tidal currents is insufficient to ensure an accurate bed stress determination.

The spatial distribution of the M_4 tide computed with the model is in reasonable agreement with observations; an accurate reproduction of this component, particularly the M_4 tidal currents in nearshore regions, is enhanced by the finer grid resolution. The M_4 tidal currents in the near-bed region are influenced by viscous and bottom friction effects and the inclusion of the advective terms.

The M_6 component of the tide shows significantly larger spatial variability than that found for the M_4 components, although with the high grid resolution of the present model it should be possible to resolve this component. A detailed comparison with observations was, however, rather inconclusive; this may in part be due to possible errors in the observations. Another reason may be that, because the M_6 tide is produced by the nonlinear friction term, which is influenced by other tidal constituents, such as S_2, N_2, K_1, and O_1 that are significant in the area (Davies and Jones 1992) and were not included, bottom frictional effects may have been underestimated (detailed calculations to examine this possibility are presently in progress.)

Tidal residuals computed with the omission of the advective terms show small tidal residual flows in offshore regions, with strong flows in the shallow nearshore areas. Including the advective terms increases the magnitude of the tidal residuals in offshore areas, particularly in the region to the east of the Isle of Man, where tidal currents are strong and change direction quite rapidly. The significant differences between depth mean and near-bed tidal residuals suggests that for problems such as sediment transport where the near-bed residual flow is important, it is necessary to consider the bed residual.

Acknowledgments. The authors are indebted to R. A. Smith and J. Campbell for assistance in preparing figures and J. Hardcastle and L. Parry for typing the paper.

REFERENCES

Aldridge, J. N., and A. M. Davies, 1993: A high-resolution three-dimensional hydrodynamic tidal model of the eastern Irish Sea. *J. Phys. Oceanogr.*, **23,** 207–224.

Blumberg, A. F., and G. L. Mellor, 1987: A description of a three-dimensional coastal ocean circulation model. *Three-Dimensional Coastal Ocean Models,* N. S. Heaps, Ed., Coastal and Estuarine Sciences, No. 4, Amer. Geophys. Union, 1–16.

Crawford, W. R., 1991: Tidal mixing and nutrient flux in the waters of southwest British Columbia. *Tidal Hydrodynamics,* B. B. Parker, Ed., John Wiley and Sons, 855–872.

Davies, A. M., 1986: A three-dimensional model of the northwest European continental shelf with application to the M_4 tide. *J. Phys. Oceanogr.*, **16,** 797–813.

——, 1987: Spectral models in continental shelf sea oceanography. *Three-Dimensional Coastal Ocean Models,* N. S. Heaps, Ed., Coastal and Estuarine Sciences, No. 4, Amer. Geophys. Union, 71–106.

——, 1990: On the importance of time varying eddy viscosity in generating higher tidal harmonics. *J. Geophys. Res.,* **95,** 20 287–20 312.

——, 1991: On using turbulence energy models to develop spectral viscosity models. *Contin. Shelf Res.,* **11,** 1313–1353.

——, 1993: A bottom boundary layer-resolving three-dimensional tidal model: A sensitivity study of eddy viscosity formulation. *J. Phys. Oceanogr.,* **23,** 1437–1453.

——, and J. E. Jones, 1990: Application of a three-dimensional turbulence energy model to the determination of tidal currents on the northwest European shelf. *J. Geophys. Res.,* **95,** 18 143–18 162.

——, and ——, 1992: A three-dimensional model of the M_2, S_2, N_2, K_1 and O_1 tides in the Celtic and Irish Seas. *Progress in Oceanography,* Vol. 29, Pergamon, 197–234.

——, and H. Gerritsen, 1994: An intercomparison of three-dimensional tidal hydrodynamic models of the Irish Sea. *Tellus,* **46A**(2), 200–221.

——, and J. Lawrence, 1994: A three-dimensional model of the M_4 tide in the Irish Sea: The importance of open boundary conditions and influence of wind. *J. Geophys. Res.,* **99,** 16 197–16 227.

Flather, R. A., and K. P. Hubbert, 1990: Tide and surge models for shallow water—Morecambe Bay revisited. *Modeling Marine Systems,* Vol. 1, A. M. Davies, Ed., CRC Press, 135–166.

Foreman, M. G. G., and R. A. Walters, 1990: A finite-element tidal model for the southwest coast of Vancouver Island. *Atmos.–Ocean,* **18,** 261–287.

——, R. F. Henry, R. A. Walters, and V. A. Ballantyne, 1993: A finite element model for tides and resonance along the north coast of British Columbia. *J. Geophys. Res.*, **98,** 2509–2531.

Gordon, R. B., and M. L. Spaulding, 1987: Numerical simulations of the tidal- and wind-driven circulation in Narragansett Bay. *Estuar. Coastal Shelf Sci.*, **24,** 611–636.

Green, M. O., J. M. Rees, and N. D. Pearson, 1990: Evidence for the influence of wave–current interaction in a tidal boundary layer. *J. Geophys. Res.*, **95,** 9629–9644.

Heaps, N. S., and J. E. Jones, 1981: Three-dimensional model for tides and surges with vertical eddy viscosity prescribed in two layers. II, Irish Sea with bed friction layer. *Geophys. J. Roy. Astron. Soc.*, **64,** 303–320.

Howarth, M. J., 1990: Atlas of tidal elevations and currents around the British Isles. Department of Energy, Offshore Technology Rep. OTH 89 293, 16 pp.

Johns, B., and J. Xing, 1993: Three-dimensional modelling of the free-surface turbulent flow of water over a bed form. *Contin. Shelf Res.*, **13,** 705–723.

——, P. Marsaleix, C. Estournel, and R. Vehil, 1992: On the wind-driven coastal upwelling in the Gulf of Lions. *J. Mar. Syst.*, **3,** 309–320.

Lohrmann, A., B. Hackett, and L. P. Roed, 1990: High resolution measurements of turbulence, velocity and stress using a pulse-to-pulse coherent sonar. *J. Atmos. Oceanic Technol.*, **7,** 19–37.

Luyten, P. J., E. Deleersnijder, K. G. Ruddick, and J. Ozer, 1996: Presentation of a family of turbulence closure models for stratified shallow water flows and preliminary application to the Rhine outflow region. *Contin. in Shelf Res.*, **16,** 101–130.

Lynch, D. R., and F. E. Werner, 1990: Three-dimensional hydrodynamics on finite elements. Part II: Nonlinear time-stepping model. *Int. J. Numer. Methods Fluids,* **12,** 507–534.

——, and ——, 1991: Three-dimensional velocities from a finite-element model of English Channel/Southern Bight tides. *Tidal Hydrodynamics,* B. B. Parker, Ed., John Wiley and Sons, 183–200.

——, and C. E. Naimie, 1993: The M_2 tide and its residual on the outer banks of the Gulf of Maine. *J. Phys. Oceanogr.*, **23,** 2222–2253.

Pugh, D. T., and J. M. Vassie, 1976: Tide and surge propagation offshore in the Dowsing Region of the North Sea. *Dtsch. Hydrogr. Z.*, **29,** 163–213.

Robinson, I. S., 1979: The tidal dynamics of the Irish and Celtic Seas. *Geophys. J. Roy. Astron. Soc.*, **56,** 159–197.

Schwiderski, E. W., 1986: Worldwide ocean tide modelling. *Advanced Physical Oceanographic Numerical Modelling,* J. J. O'Brien, Ed., NATO ASI Series, Springer-Verlag, 329–372.

Spaulding, M. L., 1984: A vertically averaged circulation model using boundary fitted coordinates. *J. Phys. Oceanogr.*, **14,** 973–982.

Uncles, R. J., 1991: M_4 tides in a macrotidal, vertically mixed estuary: The Bristol Channel and Severn. *Tidal Hydrodynamics,* B. B. Parker, Ed., John Wiley and Sons, 341–355.

Werner, F. E., and D. R. Lynch, 1989: Harmonic structure of English Channel/Southern Bight tides from a wave equation simulation. *Adv. Water Resour.*, **12,** 121–142.